Analysis of meiosis in *Pristionchus pacificus* reveals plasticity in homolog pairing and synapsis within the nematode lineage

Regina Rillo-Bohn[1,2,3,4], Renzo Adilardi[1,2,3,4], Barış Avşaroğlu[1,2,3,4], Lewis Stevens[5], Simone Köhler[1,2,3,4,6], Joshua Bayes[1,2,3,4], Clara Wang[1,2,3,4], Sabrina Lin[1,2,3,4], Kayla Baskevitch[1,2,3,4], Abby F. Dernburg[1,2,3,4]

[1]Department of Molecular and Cell Biology, University of California, Berkeley, Berkeley, CA United States; [2]Howard Hughes Medical Institute, Chevy Chase, MD United States; [3]Biological Systems and Engineering Division, Lawrence Berkeley National Laboratory, Berkeley, CA United States; [4]California Institute for Quantitative Biosciences, Berkeley, CA United States; [5]Institute of Evolutionary Biology, University of Edinburgh, Edinburgh, UK; [6]Cell Biology and Biophysics Unit, European Molecular Biology Laboratory, Heidelberg, Germany

ABSTRACT

The goal of meiosis is to produce haploid gametes from diploid progenitor cells. While meiosis was likely present in the last eukaryotic common ancestor (LECA), diversity in meiotic mechanisms has long been observed among sexually reproducing eukaryotes. Here we describe a new, comparative model system for molecular analysis of meiosis, the nematode *Pristionchus pacificus*, a distant relative of the widely studied model organism *Caenorhabditis elegans*. Despite superficial similarities in germline organization and meiotic progression between *P. pacificus* and *C. elegans,* we identify fundamental differences in the molecular mechanisms underlying homolog pairing, synapsis, and crossover regulation. Whereas *C. elegans* has lost the meiosis-specific recombinase Dmc1, *P. pacificus* expresses both DMC-1 and RAD-51, which localize sequentially to meiotic chromosomes during prophase. We find that *Ppa-spo-11* and *Ppa-dmc-1* are required for stable homolog pairing, synapsis, and crossover formation, while *Ppa-rad-51* is dispensable for these key processes during early prophase and plays a supporting role in meiotic double-strand break repair. Additionally, we show that elevated crossover recombination in *P. pacificus* likely arises through a Class II pathway normally inactive in *C. elegans*, shedding light on crossover control and the evolution of recombination rates.

INTRODUCTION

All sexually reproducing organisms rely on the specialized cell division process of meiosis to generate haploid gametes from diploid precursors. Upon fertilization, haploid gametes fuse and restore the diploid chromosome complement in the zygote. Thus, meiosis is essential for the survival of sexually reproducing species.

A defining feature of meiosis is a "reductional" segregation in which homologous chromosomes are separated, usually during the first of two nuclear divisions. A highly choreographed series of chromosome transactions precedes this division and ensures faithful homolog segregation: (1) pairing, in which chromosomes contact and recognize their homologous partners; (2) synapsis, defined as the assembly of a protein ensemble called the synaptonemal complex (SC) between homologs, which leads to their lengthwise alignment; and (3) crossover (CO) recombination, which creates physical linkages between chromosomes that promote proper bi-orientation during anaphase I. Failure to form at least a single CO between paired homologs results in nondisjunction and aneuploid gametes (Zickler and Kleckner, 1999).

Although pairing, synapsis and CO recombination are nearly ubiquitous among eukaryotes, details of these mechanisms show remarkable diversity among different lineages. In most model fungi, plants, and animals, stable homologous chromosome pairing and synapsis depend on early steps of the recombination pathway. Meiotic recombination is initiated by a conserved topoisomerase-like enzyme called Spo11, which catalyzes programmed DNA double-strand breaks (DSBs) across the genome, a subset of which are ultimately processed into COs (Keeney, 2008; Keeney et al., 1997). DSBs are resected to form 3' single-stranded DNA overhangs. Dmc1, a meiosis-specific recombinase, forms filaments along these ssDNA segments and promotes interhomolog strand invasion. Spo11-dependent induction of DSBs and Dmc1-dependent strand invasion are crucial for proper pairing and synapsis in the budding yeast *Saccharomyces cerevisiae*, the flowering plant *Arabidopsis thaliana,* and mammalian

model *Mus musculus* (Bishop et al., 1992; Couteau et al., 1999; Grelon, 2001; Pittman et al., 1998; Rockmill et al., 1995; Yoshida et al., 1998).

In contrast, recombination-independent mechanisms of pairing and synapsis have been characterized in other prominent model systems, including the dipteran *Drosophila melanogaster* and the nematode *Caenorhabditis elegans*. While recombination is essential for successful execution of meiosis in *C. elegans* and in female fruit flies, homolog pairing and synapsis can be uncoupled from early recombination events. During female meiosis in *D. melanogaster*, pairing initiates in proliferating germline stem cells before oocytes enter meiosis (Christophorou et al., 2013; Joyce et al., 2013; Rubin et al., 2016) and is stabilized by SC formation. *D. melanogaster* males lack recombination and SCs, and have apparently evolved a distinct mechanism to stabilize homolog pairing and enable reductional segregation (McKee et al., 2012). In *C. elegans*, pairing and synapsis are driven by Pairing Centers, specialized sites on each chromosome bound by a family of zinc-finger proteins that mediate nuclear envelope attachment and chromosome dynamics (MacQueen et al., 2005; Phillips et al., 2005; Phillips and Dernburg, 2006; Sato et al., 2009). While nuclear envelope attachment and chromosome movement play important roles in meiotic pairing and synapsis across eukaryotes, in *C. elegans* they have acquired a critical role in coupling homolog pairing to synapsis initiation (Penkner et al., 2009; Sato et al., 2009).

To investigate how the meiotic program is modified during evolution, we have established tools to investigate meiosis in the free-living nematode *Pristionchus pacificus.* Like its distant relative *C. elegans*, *P. pacificus* is an androdioecious species, characterized by a population of mostly self-fertilizing hermaphrodites (XX) and a low frequency of males (XO) (Sommer et al., 1996). Like *C. elegans, P. pacificus* has a short life cycle of 3.5 days, produces large broods of about 200 progeny by self-fertilization, and is easily cultured in the lab (Hong and Sommer, 2006). Although *C. elegans* and *P. pacificus* diverged an estimated 200-300 million years ago (Pires-daSilva, 2004), they share the same number of chromosomes (2n=12) and, with the exception of one major chromosomal translocation, macrosynteny is maintained between the two species (Dieterich et al., 2008; Rödelsperger et al., 2017). *P. pacificus* has been established as a model for comparative studies in development, evolution and ecology

(Sommer, 2015). Recent improvements in the genome assembly (Rödelsperger et al., 2017) and advances in genome editing (Lo et al., 2013; Namai and Sugimoto, 2018; Witte et al., 2015) have facilitated investigation of cell biological processes at a more mechanistic level.

In addition to these general features that make *P. pacificus* a tractable model system, previous studies revealed interesting variations from *C. elegans.* First, genome sequencing revealed the presence of the Dmc1 gene, which is absent from the entire *Caenorhabditis* clade (Figure 2 - Supplement 1 and Dieterich et al., 2008). Loss of Dmc1 correlates with the adaptation of recombination-independent mechanisms for pairing and synapsis in *Drosophila* and *Caenorhabditis* (Villeneuve and Hillers, 2001). Therefore, it was of great interest to us to examine how homologous chromosomes pair and synapse in the presence of Dmc1. Second, genetic linkage maps have revealed that multiple crossovers typically occur per chromosome pair during meiosis in *P. pacificus* (Srinivasan et al., 2003, 2002). This is in striking contrast to *C. elegans,* which exhibits complete crossover interference; only a single Class I CO normally occurs per chromosome pair (Martinez-Perez and Colaiácovo, 2009). These observations suggest a major difference in the mechanism of crossover control between these two species.

By employing CRISPR/Cas9-mediated genome editing techniques, genetics, immunocytochemistry and microscopy, we describe here the early events of meiotic prophase in *P. pacificus*. We show that homolog pairing, synapsis and CO recombination are dependent on *Ppa-spo-11* and *Ppa-dmc-1*, while *Ppa-rad-51* is not essential for meiosis. We also provide evidence that a single Class I crossover occurs per homolog pair in *P. pacificus*, implying that the higher recombination rate is due to Class II crossovers. Our work establishes tools for future investigation and highlights the flexibility of the meiotic program within the nematode lineage.

RESULTS

P. pacificus as a comparative model system for meiosis

The morphology and organization of the *P. pacificus* germline is superficially very similar to that of *C. elegans*. Hermaphrodites have two gonad arms in which sperm and ova are produced sequentially,

while males have a single arm (Rudel et al., 2005). DAPI staining of adult hermaphrodite gonads reveals a cylindrical monolayer of cells; the distal tip is populated by proliferating germline stem cells (Figure 1A-C). As germ cells enter meiosis, their nuclear morphology abruptly becomes asymmetrical, as the chromosome mass adopts a conspicuous, crescent-shaped morphology (Figure 1A). Immediately proximal to this "transition zone," DAPI staining reveals parallel tracks, indicative of paired and synapsed homologous chromosomes in the pachytene stage. Oocyte chromosomes in *P. pacificus* undergo a dramatic decondensation between diplotene and diakinesis, a stage that has been referred to as the "growth zone" (Rudel et al., 2005) or "diffuse stage" (Zickler and Kleckner, 1999). Similar diffuse chromosome morphology is observed during late prophase in other eukaryotes, but is rarely seen in *C. elegans*. As oocytes mature in the proximal region of the hermaphrodite gonad, they form a single row of large cells, and chromosomes condense dramatically. Six bivalents can be detected as compact DAPI-staining bodies during diakinesis, the stage preceding the first meiotic division, during oogenesis (Figure 1A, Sommer et al., 1996, Rudel et al., 2005).

It has been assumed that chromosomes in *P. pacificus* are holocentric, as in *C. elegans*, but we are unaware of direct evidence to support this idea. We thus identified a gene encoding CENP-C (*hcp-4* in *C. elegans*), a conserved kinetochore protein, in the *P. pacificus* genome and inserted a V5 epitope tag at its 3' end using CRISPR/Cas9. The appearance of mitotic chromosomes in embryos and in the premeiotic germline confirmed their holocentric organization (Figure 1C). Ppa-CENP-C::V5 forms linear structures, a hallmark of holocentric chromosomes, instead of discrete foci as observed for monocentric chromosomes.

Stable homolog pairing requires early recombination factors

BLAST searches of the *P. pacificus* genome revealed an open reading frame encoding an unambiguous ortholog of Dmc1, a meiosis-specific paralog of Rad51 (Table S1). An ortholog of the Dmc1 cofactor Mnd1 was also readily identified; although its partner Hop2 was not apparent among the predicted proteins or published nucleotide sequence (Figure 2 – Supplement 1). By contrast,

Dmc1/Mnd1/Hop2 are absent from both *C. elegans* and *D. melanogaster*, two model organisms that have evolved recombination-independent mechanisms of homolog pairing and synapsis (Villeneuve and Hillers, 2001). We analyzed the genome sequences of other nematodes to determine the evolutionary history of these genes within the nematode lineage (Bolt et al., 2018; https://parasite.wormbase.org). This analysis revealed that Dmc1/Mnd1/Hop2 have been lost several times during the evolution of nematodes, including the entire *Caenorhabditis* genus and all sequenced members of Clade IV (Figure 2 – Supplement 1). Not surprisingly in light of its essential function in DNA repair, the recombinase Rad51 was detected in almost all genomes with the exception of *Haemonchus contortus, Parascaris univalens* and *Parascaris equorum* (data not shown). It is likely that the absence of Rad51 orthologs reflects incomplete genome assembly and/or annotation.

Our analysis also identified homologs of four related zinc finger proteins required for pairing center activity in *C. elegans* (HIM-8, ZIM-1, ZIM-2, and ZIM-3) in most of the genome sequences from Clade V. Thus, many species within this clade have genes encoding both pairing center proteins and Dmc1/Mnd1/Hop2, but *Caenorhabditids* have lost the latter while *Pristionchus* apparently diverged before the emergence of the former.

We tested whether homolog pairing in *P. pacificus* is dependent on these early recombination factors. To generate *spo-11*, *dmc-1* and *rad-51* null mutants, we employed TALEN-mediated gene disruption, and later CRISPR/Cas9 genome editing techniques (this study; Lo et al., 2013; Witte et al., 2015). Methods such as co-CRISPR that facilitate detection of genome editing events have not worked consistently in our hands (data not shown). Nevertheless, we were able to isolate mutant alleles by screening a large number of F1 progeny from injected hermaphrodites (see Materials and Methods). Independent alleles isolated from either TALEN or CRISPR-mediated genome editing resulted in identical mutant phenotypes. All data presented here were based on alleles generated by CRISPR/Cas9. Because balancer chromosomes are not currently available for *P. pacificus*, most mutations described here were maintained in unbalanced heterozygotes, which were identified by PCR-based genotyping. Self-fertilization of heterozygotes results in broods with 25% homozygous mutant animals.

As expected, disruption of either *spo-11* or *dmc-1* resulted in the detection of 12 DAPI-staining univalent chromosomes at diakinesis, indicative of a failure in CO recombination (Figure 5). Surprisingly, *rad-51* mutants showed only mild meiotic defects (see below), and we thus confirmed the loss of RAD-51 function in mutant animals by generating multiple alleles, and confirming the absence of RAD-51 by immunofluorescence using a polyclonal antibody against Ppa-RAD-51 (Figure 4 – Supplement 1A, see Materials and Methods). Mutations in *spo-11* and *dmc-1,* but not *rad-51,* also resulted in an obvious extension of the region of the germline displaying the crescent-shaped nuclear morphology characteristic of early meiosis (Figure 2 – Supplement 2). A similar "extended transition zone" phenotype is seen in *C. elegans* mutants that fail to synapse their chromosomes during meiosis, suggesting that *spo-11* and *dmc-1* might be required for synapsis in *P. pacificus*.

To visualize and quantify homolog pairing, we generated FISH probes against two short tandem repeats found on Chromosome X and IV (Figure 2A). We measured the distance between pairs of homologous FISH signals in individual nuclei for each genotype. To analyze pairing kinetics, we divided the distal gonads into five zones of equal length. In zone 1, which mostly consists of proliferating germ cells, pairs of FISH signals remained far apart, with an average distance of 2.4 ± 1.0 μm (SD) and 2.5 ± 0.8 μm for Chrom X and IV, respectively (Figure 2B, D). In zone 2, which spans the transition zone, the average distances decreased significantly in wild-type animals (1.2 ± 1.1 μm and 1.1 ± 1.1 μm for Chrom X and IV, respectively), and homologous signals remained closely associated in the subsequent meiotic stages. Notably, homologous FISH probes localized closer together, on average, in the two zones immediately following meiotic entry, and showed some separation in zones 4 and 5 (Figure 2B, D). By contrast, in wild-type *C. elegans*, homologous loci remain closely apposed in most of the distal region of the gonad (MacQueen et al., 2002). Together with analysis of synapsis (below), this indicated that desynapsis initiates shortly after completion of synapsis in *P. pacificus*, resulting in partial separation of homologs.

We noted that the average distances between pairs of homologous FISH signals in *spo-11* and *dmc-1* mutants also decreased markedly upon meiotic entry, although clearly less so than in wild type

(Figure 2D). In contrast, *rad-51* mutants showed distributions of probe distances similar to wild-type animals (Figure 2C, D). We considered the possibility that the proximity between FISH signals might reflect the clustering of all chromosomes within a subregion of the nucleus, which is apparent during the "transition zone" (leptotene/zygotene), rather than specific homologous interactions. If so, the extended transition zone morphology in *spo-11* and *dmc-1* might obscure a pairing defect that would be more apparent in the absence of clustering (Figure 2 – Supplement 2). To address this, we measured the distances between pairs of heterologous FISH signals in the premeiotic region (dispersed) versus the transition zone (clustered). We observed that heterologous FISH signals were also significantly closer to each other in the transition zone compared to premeiotic nuclei in both wild-type and mutant animals (Figure 2E). Furthermore, the distances between heterologous versus homologous pairs of FISH loci were not significantly different in *spo-11* and *dmc-1* mutants ($p=0.1777$ and $p=0.6774$, respectively, by Student's *t*-test), but were clearly different in wild-type meiocytes ($p<0.0001$ by Student's *t*-test) (Figure 2E). These data support the idea that clustering, rather than specific pairing, promote proximity between these loci during leptotene/zygotene in *spo-11* and *dmc-1* mutants. Although we cannot conclude that transient homologous pairing is absent in these mutants, it is evident that these early recombination factors are required for stable pairing and extended association of homologous loci throughout prophase. In contrast, *rad-51* is dispensable for homolog pairing, as in *C. elegans*.

SPO-11 and DMC-1 are required for homologous synapsis

To further investigate meiotic progression in *P. pacificus* and to probe the role of early recombination factors in synapsis, we developed cytological markers for the chromosome axis, which normally assembles upon meiotic entry, and the synaptonemal complex (SC), which assembles between paired axes during early prophase. Identification of a candidate axial element component was straightforward, due to the presence of the easily recognized HORMA (Hop1, Rev7, Mad2) domain among members of this family of proteins (Aravind and Koonin, 1998; Vader and Musacchio, 2014). We identified a gene encoding a HORMA domain protein that is most closely related to *Cel-him-3* by

reciprocal BLAST analysis (Table S1). We refer to this gene as *Ppa-hop-1*, after the founding member of the meiotic HORMA proteins, *S. cerevisiae* Hop1. We raised a polyclonal antibody by genetic immunization using a fragment that encodes a peptide of 100 amino acids in length, including part of the HORMA domain, and found that this antibody indeed recognized chromosome axes from meiotic entry through late pachytene.

To enable cytological detection of synaptonemal complex (SC) assembly, we searched for homologs of SC proteins. This is notoriously challenging due to rapid divergence of these proteins, and their extensive regions of coiled-coil potential, which is associated with a strongly skewed amino acid composition. *C. elegans* expresses four known SC proteins, known as SYP-1, SYP-2, SYP-3, and SYP-4 (Colaiácovo et al., 2003; MacQueen et al., 2002; Smolikov et al., 2009, 2007). SYP-4 contains a distinctive C-terminal domain with several unusual motifs enriched in glycine and phenylalanine residues. We generated and sequenced an RNA library from isolated gonads, which facilitated identification of full-length *Ppa-syp-4*. We inserted an HA epitope tag at the C-terminus of the coding sequence via template-directed repair of a CRISPR/Cas9-induced break, and found that immunofluorescence with an epitope-specific antibody localized specifically between paired meiotic chromosomes, confirming SYP-4-HA as a marker for the SC (Figure 3A, B). The tagged protein supported normal meiosis, demonstrated by the low percentage of inviable embryos and males in the strain population (Figure 3 – Supplement 1).

HOP-1 was detected in the nucleoplasm in the premeiotic region of the germline and formed linear structures along chromosomes upon meiotic entry. SYP-4 was detected along chromosome segments shortly thereafter, and fully colocalized with HOP-1 tracks during pachytene. Notably, the region of the germline containing nuclei with fully aligned stretches of SYP-4 and HOP-1 was very short compared to *C. elegans,* in which SC disassembly occurs close to the bend of the gonadal arm, shortly prior to diakinesis. In contrast, SC disassembly initiated much earlier in *P. pacificus*; the major fraction of prophase nuclei is best described as “pachy-diplotene,” since chromosomes remain only partially synapsed. Six short stretches of SYP-4 were apparent in these nuclei, and persisted over an extended region (Figure 3A, B). This asymmetrical pattern of the SC is highly reminiscent of a more transient stage

in *C. elegans*, in which the SC remains associated with the "short arm" of each homolog pair and subsequently contributes to the step-wise loss of cohesion during the first and second meiotic divisions (Lui and Colaiácovo, 2012).

HOP-1 localized normally to chromosome axes in *spo-11* and *dmc-1* mutants, but extensive SC assembly failed. Instead, small, dispersed puncta of SYP-4 were observed along chromosome axes, with occasional longer tracks (Figure 3C). In contrast to *spo-11* and *dmc-1* mutants, *rad-51* mutants displayed robust synapsis with a distribution of stages similar to that seen in wild-type hermaphrodites (Figure 3C). These observations indicate that *spo-11* and *dmc-1* play crucial roles during homologous synapsis in *P. pacificus,* while *rad-51* is dispensable for this process. This further suggests that synapsis initiation may be tightly coupled to homolog pairing and that SPO-11 and DMC-1, but not RAD-51, play central roles in this process.

DMC-1 and RAD-51 localize sequentially during distinct stages of meiotic prophase

To investigate the functions of and interplay between DMC-1 and RAD-51 in *P. pacificus*, we inserted a V5 epitope tag at the C-terminus of the *Ppa-dmc-1* coding sequence via CRISPR/Cas9 and raised a polyclonal antibody that recognizes Ppa-RAD-51 (see Materials and Methods). DMC-1::V5 supported normal meiosis, as evidenced by a normal brood size, high embryonic viability and low percentage of males (Figure 3 – Supplement 1). Surprisingly, the two proteins showed distinct and nonoverlapping patterns of localization. DMC-1 localized broadly on chromatin in transition zone nuclei and disappeared immediately upon completion of synapsis. RAD-51 displayed a much more restricted, punctate distribution along chromosomes, and was only detected in nuclei in which DMC-1 no longer coated the chromatin (Figure 4A, B). Occasional nuclei at the border between the transition zone and pachytene region exhibited both DMC-1 and RAD-51, although DMC-1 was very faint in these nuclei and did not overlap with RAD-51 (Figure 4C). Additionally, DMC-1 remained strongly associated with chromosomes in some late nuclei that retained clustered DAPI morphology, presumably either "straggler"

cells that were delayed in complete synapsis or crossover designation, or were undergoing apoptosis (Figure 4D).

We also tested the interdependence of DMC-1 and RAD-51 recombinases for their localization. In *S. cerevisiae* and *A. thaliana*, Dmc1 functions as an essential catalyst for interhomolog joint molecule formation during meiotic DSB repair, while Rad51 acts as an accessory protein for proper Dmc1 nucleofilament formation (Cloud et al., 2012; Da Ines et al., 2013). We did not detect RAD-51 along chromosomes in the transition zone, where DMC-1 was abundant on chromatin, and we found that DMC-1::V5 was normal in *rad-51* mutants, indicating that RAD-51 does not play an essential role in the recruitment of DMC-1 (Figure 4 – Supplement 1A). Conversely, RAD-51 was also observed in some nuclei in *dmc-1* mutants, specifically in late prophase nuclei proximal to the extended transition zone (Figure 4 – Supplement 1B). RAD-51 foci were both more abundant and larger in *dmc-1* mutants compared to wild-type pachytene nuclei, perhaps due to persistent unrepaired DSBs that accumulate in the absence of DMC-1 protein. Alternatively, the bright foci of RAD-51 observed in late prophase nuclei could be indicative of an apoptotic response to unrepaired breaks and/or extensive asynapsis.

In *spo-11* mutants, which are expected to lack any meiotic DSBs, DMC-1 failed to localize to chromosomes, and instead formed nuclear aggregates (Figure 4 – Supplement 1C). It was unclear whether these DMC-1 aggregates were bound to chromatin. Since DMC-1 does not appear to bind specifically at recombination intermediates in wild-type nuclei, this suggests that the absence of DMC-1 reflects a *spo-11*–dependent regulatory mechanism, likely through activation of a DNA damage signaling pathway, rather than an absence of potential binding sites. Consistent with cytological evidence that RAD-51 localizes specifically with recombination intermediates, the protein was absent from chromosomes in *spo-11* mutants during meiotic prophase (Figure 4 – Supplement 1E). Detection of RAD-51 foci in the premeiotic region of *spo-11* mutants provides a positive control for immunofluorescence (Figure 4 – Supplement 1D). Thus, our data show that DMC-1 and RAD-51 bind to chromatin at different stages of meiotic prophase and are not interdependent, although both require DSBs for their localization.

RAD-51 is not required for crossover formation or completion of meiosis

To assess the roles of DMC-1 and RAD-51 in crossover formation, we quantified the number of DAPI-staining bodies at diakinesis in *dmc-1* and *rad-51* mutants. Wild-type oocytes at this stage contained ~6 DAPI-staining bodies (average= 5.6), as expected, while in *spo-11* mutants, ~12 DAPI-staining bodies were present (average= 11.5), consistent with a complete failure of crossover formation in the absence of DSBs (Figure 5A,B). Interestingly, in *dmc-1* mutant germlines we frequently failed to detect oocytes at diakinesis, indicative of a defect in meiotic progression and the likely activation of a checkpoint in response to unrepaired DSBs. In cases when we did observe nuclei at diakinesis, they contained an average of 11.6 DAPI-staining bodies, reflecting a complete absence of crossovers as in *spo-11* mutants (Figure 5C, D).

Somewhat surprisingly, disruption of *rad-51* resulted in homozygous hermaphrodites that were viable and fertile, although animals produced smaller broods and their embryos showed greatly reduced viability (Figure 5E). Homozygous *rad-51* mutant gonads also displayed diakinesis nuclei more frequently than *dmc-1* mutants, although they were absent in 2 out of 20 gonads scored, indicating that loss of DMC-1 function impairs meiotic progression more severely than loss of RAD-51 (Figure 5C, D). Consistent with this observation, while *rad-51* mutants had a lower average brood size compared to wild-type animals, *dmc-1* mutants had even smaller broods, ranging from zero to 35 embryos laid per mutant homozygote (Figure 5E). In striking contrast to *Cel-rad-51* mutants, which display fragmented chromatin aggregates at diakinesis (Martin et al., 2005; Rinaldo et al., 2002), *Ppa-rad-51* mutants displayed an average of 6 DAPI-staining bodies, similar to wild-type (Figure 5B). Together with the relatively high viability of progeny of *rad-51* homozygous mutants, this indicates that RAD-51 does not play an essential role in crossover formation in *P. pacificus.*

Conserved crossover factor COSA-1 marks Class I COs in *P. pacificus*

To further analyze crossover formation in *P. pacificus*, we identified the gene encoding the metazoan meiotic cyclin-related protein COSA-1/Cntd1 and inserted a 3xFLAG epitope tag at the C-

terminus of the coding sequence via CRISPR/Cas9. The strain expressing COSA-1::3xFLAG yielded progeny with high embryonic viability and low percentage of males, demonstrating that the tagged protein functions sufficiently to support normal meiosis (Figure 3 – Supplement 1). Immunostaining with anti-FLAG antibodies revealed discrete foci along the SC, beginning as early as zygotene, which decreased in number and became more intense during the brief pachytene region (Figure 6A, B). Most pachytene nuclei displayed 6 COSA-1 foci, each of which was associated with an individual SC between each pair of homologous chromosomes (Figure 6C and Supplementary Video 1). Previous genetic mapping experiments revealed that homolog pairs often experience multiple crossovers in *P. pacificus* (Srinivasan et al., 2002). To investigate whether these extra crossovers might arise specifically during spermatogenesis, we analyzed younger J4 hermaphrodites whose germlines had not yet undergone the switch from spermatogenesis to oogenesis, which occurs in early adulthood, and found that pachytene nuclei undergoing spermatogenesis also displayed ~6 COSA-1 foci (Figure 6- Supplemental Figure 1). This suggests that *P. pacificus*, like *C. elegans*, exhibits complete chromosome-wide Class I CO interference and, combined with previous genetic data, implies that additional crossovers likely arise through the Class II CO pathway, which does not require COSA-1.

Intriguingly, SC disassembly appeared to be regulated by the position of the lone Class I CO between each chromosome pair, as in *C. elegans*. By mid-pachy-diplotene, 6 short stretches of SYP-4::HA were observed, each associated with a single COSA-1::3xFLAG focus near one end (Figure 6B). During late pachy-diplotene, COSA-1::3xFLAG foci were no longer visible, although short stretches of SYP-4::HA could still be observed. A major difference from *C. elegans* that occurs in *P. pacificus* during SC disassembly is the visible splaying of chromosome axes upon removal of the central element component(s) (Figure 6D). HOP-1 is retained on the axes upon disassembly of the SC though the signal is more difficult to visualize as two separate axial structures. At this stage, short stretches of SYP-4::HA colocalize with corresponding bright stretches of HOP-1 (Figure 3B and Figure 6D). Bivalents at diakinesis also show a cruciform structure similar to that seen in *C. elegans*, indicative that only the Class I crossovers give rise to chiasmata that persist until diakinesis.

We next looked at the pattern of COSA-1::3xFLAG in various mutant backgrounds. As expected, *dmc-1* mutants showed a complete absence of COSA-1 foci throughout prophase, while 6 foci were readily observed during pachytene in *rad-51* mutants (Figure 7A). These observations were consistent with the number of DAPI-staining bodies we observed in diakinesis (Figure 5B). Surprisingly, a few bright COSA-1::3xFLAG foci were present throughout prophase in *spo-11* mutants (Figure 7A). However, since ~12 DAPI-staining bodies were observed during diakinesis, we conclude that these COSA-1 foci do not mark designated COs. A similar phenomenon has been reported in *C. elegans spo-11* mutants (Nadarajan et al., 2017; Pattabiraman et al., 2017), suggesting that COSA-1 can coalesce at sites lacking bona fide recombination intermediates.

DISCUSSION

Distinct roles of Dmc1 and Rad51

Rad51 and Dmc1 show very similar activities *in vitro*, but these proteins clearly play non-redundant functions in meiosis. This is at least in part due to the activity of Dmc-1 specific cofactors, as well as differential regulation of the timing and activities of the two paralogs. Our analysis of the two RecA homologs in *P. pacificus,* RAD-51 and DMC-1, defines their distinct contributions during meiosis.

The pattern of extensive DMC-1 loading in transition zone nuclei is not likely to reflect an exorbitant number of DSBs or recombination intermediates present in the genome. Instead we favor the idea that DMC-1 or its cofactors is specifically regulated at this stage to promote its nonspecific association with double-stranded DNA or chromatin, and that this regulation depends on *spo-11* activity. Purified yeast and human Dmc1 protein are capable of binding both ssDNA and dsDNA *in vitro*, although there is a strong preference for ssDNA binding (Hong et al., 2001; Li et al., 1997; Masson et al., 1999).

The sequential localization of DMC-1 and RAD-51 first suggested that they function independently, and this is supported by our analysis of loss-of-function mutations. By contrast to budding yeast and *A. thaliana*, Ppa-RAD-51 is dispensable for the activity of DMC-1 in pairing, synapsis, and

crossover formation. Instead, RAD-51 appears to play a supporting role in DSB repair during pachytene, processing excess DSBs that remain after crossover designation has occured. In *C. elegans*, which expresses only RAD-51, a similar switch between two modes of double-strand break repair is observed during meiotic prophase (Hayashi et al., 2007). Association of Ce-RAD-51 with repair intermediates is differentially regulated from the onset of meiosis until a mid-pachytene transition that coincides with crossover designation; at this time, competence to convert DSBs to interhomolog COs is also lost. Recent work revealed an analogous switch from a "meiotic" repair to a "somatic"-like repair pathway during the transition from mid- to late pachytene in mouse spermatocytes (Enguita-Marruedo et al., 2019). In *P. pacificus,* it is thus likely that DMC-1 and RAD-51 have highly specialized functions: formation of interhomolog COs by DMC-1 in the transition zone and a more general mode of double-strand break repair by RAD-51 during pachytene. Furthermore, our observation that nuclei in *rad-51* mutants display cruciform bivalents and lack fragmented chromatin at diakinesis suggests that excess DSBs can be repaired through an alternate pathway which does not depend on RAD-51 activity, such as non-homologous end joining, or that DMC-1 can compensate for RAD-51 but not the other way around. The nature of RAD-51-dependent DSB repair and how the activities of RAD-51 and DMC-1 are regulated in early meiotic prophase will be a focus of future investigation in this species.

Crossover regulation in *P. pacificus*

Genetic mapping in *P. pacificus* revealed lengths of ~100-250 centimorgans for each chromosome, corresponding to 2-5 interhomolog crossovers per meiosis (Srinivasan et al., 2003, 2002). By contrast, the genetic map of each chromosome in *C. elegans* is 50 cM, reflecting a single crossover per pair (Hillers et al., 2017). Surprisingly, our analysis of Ppa-COSA-1 localization revealed only a single COSA-1 focus per chromosome by pachytene, very similar to what is seen in *C. elegans* (Yokoo et al., 2012). This suggests that either multiple Class I COs occur but only one retains COSA-1, or that all but a single CO forms by an alternate, COSA-1-independent pathway. In many eukaryotic systems, two CO pathways co-exist (Gray and Cohen, 2016). Class I COs show spatial interference and depend on factors

including MSH-4/5, ZHP-3/Rnf212, and COSA-1/Cntd1. On the other hand, Class II COs do not exhibit interference and undergo an alternate resolution pathway that requires the structure-specific endonuclease complex Mus81-Eme1/Mms4. In some species, notably in *A. thaliana* and *S. cerevisiae*, Class II COs can occur in the absence of Class I COs, but this may not be the case in all organisms. Future work will examine whether all COs in *P. pacificus* arise only after the single, obligate Class I CO has been designated, and whether the designation of Class I COs is necessary for the formation and resolution of Class II COs. We further note that there appears to be only one chiasma formed between each homolog pair, which is likely created by the lone COSA-1-associated Class I CO. Our work reveals the potential of *P. pacificus* to address some long-standing questions about mechanisms and regulation of crossover recombination that are not accessible in the meiotic model *C. elegans* due to the absence of Class II COs during normal meiosis.

Comparative analysis of meiosis reveals major variations within the nematode lineage

In addition to establishing key aspects of meiosis in *P. pacificus*, this work also illuminates the evolutionary history of meiosis in *C. elegans*. A body of prior work has revealed that recombination-independent homologous synapsis in *C. elegans* relies on pairing centers, specialized chromosome regions that interact with nuclear envelope and drive chromosome movement during early prophase. These meiosis-specific dynamics are typically mediated by telomeres, but have shifted to a unique region on each chromosome in *C. elegans*. Pairing centers also act as the sites of synapsis initiation (Rog and Dernburg, 2013). By contrast, in other organisms, telomere-led chromosome movement is thought to promote homologous interactions, but stabilization of pairing and initiation of synapsis occur at early recombination intermediates, which depend on Spo11 and Dmc1 activity. Pairing center activity depends on and is largely defined by the recruitment of a family of zinc finger proteins that bind to DNA sequence motifs in these regions (Phillips et al., 2009). These proteins, known as ZIM-1, ZIM-2, and ZIM-3, and HIM-8 in *C. elegans*, also act as scaffolds to recruit a cascade of kinase activities required for pairing and synapsis (Harper et al., 2011; Kim et al., 2015; Labella et al., 2011). Surprisingly, most of the sequenced

406 genomes of nematodes in Clade V include both homologs of the HIM-8/ZIM family and orthologs of
407 Dmc1, Hop2, and Mnd1 (Figure 2 – Supplement 1). The *Pristionchus* genus is unusual within this Clade
408 in that it lacks apparent homologs of the pairing center proteins, while *Caenorhabditids* are among the
409 few genera that have lost Dmc1/Mnd1/Hop2, which were independently lost along the branch leading to
410 *Oscheius tiuplae* and *Auanema rhodensis*. This suggests that the dominant role of pairing centers in
411 homologous synapsis is likely to be recently derived, perhaps restricted to *Caenorhabditids*. Future
412 analysis of species in which Dmc1 and pairing center proteins co-exist may illuminate how synapsis
413 initiation activity relocalized from sites of Dmc1-mediated strand exchange to pairing centers, and thus
414 how pairing centers acquired their central meiotic roles in *C. elegans*.

415 *C. elegans* is a popular and powerful model system for molecular studies of meiosis. *Pristionchus*
416 *pacificus* shares many of the same experimental advantages, although naturally has fewer experimental
417 tools, since it has been developed far more recently. Genome engineering using CRISPR/Cas9 is
418 somewhat more challenging, and has so far been refractory to large insertions, such as fluorescent
419 proteins. However, this barrier will likely be overcome through advances in editing efficiency. Perhaps a
420 greater obstacle is the absence of balancer chromosomes, which are invaluable for maintaining mutations
421 that reduce viability or fertility in *C. elegans*. Because balancers are unavailable for *P. pacificus*, most of
422 the mutations described in this work have been maintained in unbalanced heterozygotes through frequent,
423 labor-intensive genotyping assays. Moreover, the analysis presented here suggests that it may not be
424 possible to construct crossover-suppressing balancer chromosomes, given that recombination is essential
425 for homolog pairing and synapsis. By contrast, *C. elegans* uses a derived, recombination-independent
426 mechanism to robustly pair and synapse homologous chromosomes, which makes it possible to propagate
427 large-scale chromosome rearrangements that suppress recombination over large genomic regions while
428 maintaining regular segregation of chromosomes during meiosis.

429 The advent of broadly applicable techniques for genome editing has enabled rapid progress
430 towards developing *P. pacificus* for molecular studies, along with many other experimental models.

Future exploration of meiosis in *P. pacificus*, and perhaps in other nematode models, will further expand our understanding of core mechanisms and plasticity of sexual reproduction.

MATERIALS AND METHODS

P. pacificus *strains and maintenance*

Animals were cultured on NGM media with *E. coli* OP50 at 20°C under the same standard conditions as *C. elegans* (Brenner, 1974). The wild-type strain is a derivative of PS312 designated as "97," which was provided by Ralf Sommer. This isolate was found to be more amenable to genome editing by CRISPR-Cas9 than the parental strain. Mutant alleles were maintained in a heterozygous state. Every few generations and before each immunofluorescence or FISH experiment, single adult hermaphrodites were picked to new plates and allowed to lay embryos for two days, after which the genotype of the parent was determined by PCR genotyping. Progeny from heterozygous mothers, one-fourth of which are homozygous for the meiotic mutation, were analyzed using the assays described here; heterozygous and wild-type siblings were frequently used as controls, in addition to analysis of unedited wild-type animals.

CRISPR/Cas9 genome editing

To modify the *P. pacificus* genome, we adapted our preferred CRISPR/Cas9 protocol from *C. elegans* to *P. pacificus*. Equimolar quantities of Alt-R®CRISPR-Cas9 crRNA and tracrRNA molecules (Integrated DNA Technologies, Coralville, IA) were hybridized using a thermocycler (95°C for 5 minutes, then 25°C for 5 minutes). 4µl of 100µM hybridized tracrRNA/crRNA was combined with 4µl of 40µM *S. pyogenes* Cas9-NLS purified protein (QB3 Macrolab, UC Berkeley, Berkeley, CA) and incubated at room temperature for 5 minutes. 2µl of 100µM stock of an Ultramer® DNA oligo (IDT) repair template containing 50-60 bp homology arms and the desired epitope or mutation sequence was added to the mixture, for a total volume of 10µl, and injected into the gonads of 24 hour-post J4 adult hermaphrodites. Following a 2-4 hour recovery period, injected animals were allowed to lay embryos at

20°C for 16-20hr. Four days later, a fraction of the F1 population (typically 150-200 progeny from 6-8 injected P_0s) was screened for the presence of the mutation or epitope tag sequence by PCR genotyping, and candidate alleles were verified by Sanger sequencing. A complete list of crRNA, repair template, and genotyping primer sequences used to generate alleles in this study is provided as Table S1.

TALEN constructs were generated using a protocol adapted from Zhang et al. (2011) and designed using the TAL Effector Nucleotide Targeter 2.0 website (https://tale-nt.cac.cornell.edu/).

Viability and fertility

To quantify embryonic viability, brood size, and male progeny of wild-type and *rad-51* mutants, J4 hermaphrodites were picked onto individual plates and transferred every 24 hours over 72 hours total. Embryos were counted each day, after transferring the adult hermaphrodite to a new plate, and kept at 20°C. Three to four days later, adults were counted on each plate. To analyze *spo-11* and *dmc-1* mutants, 24 individual J4 hermaphrodites were picked from progeny of a verified heterozygous mutant hermaphrodite. Quantification was performed as in wild type, but after 72 hours, the adult hermaphrodite was lysed and genotyped for the presence of the mutation. Thus, although 24 animals total were quantified from a mixed population of *spo-11*/+ or *dmc-1*/+ animals, data from 5 homozygous *spo-11* and 7 homozygous *dmc-1* mutant animals are reported in the data table, Figure 5E.

Immunofluorescence and FISH

To stage animals for each experiment, 30-40 J4s were picked from a PCR-verified heterozygous mother onto a fresh plate and allowed to develop for an additional 24 or 48 hours at 20°C. Young adult hermaphrodites were dissected on a clean coverslip in egg buffer containing 0.05% tetramisole and 0.1% Tween-20. Samples were fixed for 2 minutes in egg buffer with 1% formaldehyde and transferred to a 1.5-ml tube containing PBST. After 5 minutes, the PBST was replaced with ice-cold methanol and incubated at room temperature for an additional 5 minutes. Worms were washed twice with PBST, blocked with Roche blocking reagent, and stained with primary antibodies diluted in Roche blocking

483 solution for 1.5-2 hours at room temperature. Samples were washed with PBST and incubated with
484 secondary antibodies raised in donkey and conjugated with Alexa-488, Cy3 or Cy5 (Jackson
485 ImmunoResearch Laboratories, West Grove, PA). Worms were then incubated with 1µg/ml DAPI in
486 PBST, washed with PBST, and mounted in ProLong™ Gold antifade mounting solution (Invitrogen)
487 before imaging.
488 For embryo staining, 20 plates of mixed-stage worms were harvested with water and treated with
489 1:8 solution of bleach:water for 5 minutes at room temperature. Embryos were collected by centrifugation
490 and washed twice with PBS. To dissolve the vitelline membrane, a solution containing 2.6 ml of n-
491 heptane, 2 ml of PBS, and 1% paraformaldehyde (final) was added to the embryo pellet for 5 minutes at
492 room temperature with shaking. Treated embryos were collected by centrifugation, washed twice with 5
493 ml MeOH, three times with PBS, and incubated with Roche blocking reagent, primary, and secondary
494 antibodies as described above. Embryos were mounted on agarose pads for imaging.
495 For FISH experiments, age-matched animals were dissected and fixed as for immunofluorescence
496 experiments described above, except that the initial fixation was for 4 minutes in 2% formaldehyde. After
497 incubation in ice-cold methanol, worms were washed with 2x SSCT twice and incubated in 50% 2x
498 SSCT/50% formamide solution overnight at 37°C. The next day, the worms were transferred to a small
499 PCR tube, excess solution was removed from the sample, and a 40 µl hybridization mix containing 250ng
500 of each probe in hybridization buffer (3.5xSSC, 58% formamide, 12.75% dextran sulfate) was added.
501 The sample was immediately denatured in a thermocycler at 91°C for 2 minutes and incubated overnight
502 at 37°C. On the last day, the worms were transferred to a 1.5-ml tube and washed with 2xSSCT. After 5
503 minutes, the solution was replaced with fresh 2xSSCT and mounted with ProLong™ Diamond Antifade
504 Mountant with DAPI (Invitrogen).
505
506 *FISH probes*
507 Probes for a central locus on chromosome IV and the left end of chromosome X were designed
508 based on two short tandem repeat motifs. Tandem Repeat Finder v4.09 (Benson, 1999) was used to

identify tandem repeats in *P. pacificus* "El Paco" genome assembly (Rödelsperger et al., 2017) using default parameters and a maximum periodicity of 200 bp. The output was then filtered to identify repeats that spanned more than 8 kb. These were compared to the genome sequence using BLAST to identify the subset of sequences restricted to a single major locus per genome. A subset of these repeats was then tested for specific and robust hybridization with oligonucleotide probes. The Chromosome IV probe targets the 30-base repeated motif TCATTGAAATGATCACAATCATTGA, which spans 40.1 kb at a position 11.3 Mb from the left end of chromosome IV. The Chromosome X probe (GGTGGTCGACGGCTGCGTCG) targets a 30-base repeat motif that spans two very close regions of 29.3kb and 11.1kb on the left end of the X chromosome. Single-stranded oligonucleotides labeled at the 3' end with 6-FAM or Cy3 dyes were purchased from IDT and used directly as FISH probes.

Antibodies

Antibodies against Ppa-RAD-51 were generated against a 6x His-tagged N-terminal fusion protein (aa 1-103) expressed and purified from bacteria. Four mice were immunized with the antigen. Serum from one animal, designated S148, was used without purification at 1:300 dilution (Pocono Rabbit Farm and Laboratory, Canadensis, PA). Antibodies against Ppa-HOP-1 were generated by genetic immunization against aa 177-276 (SDIX, Newark, DE) and used in the following experiments at 1:300 dilution. Additional antibodies were purchased from commercial sources and diluted as follows: mouse anti-FLAG (1:500, Sigma #F1804), mouse anti-V5 (1:500, Thermo Fisher #R960-25), rabbit anti-V5 (1:250, Millipore Sigma #V8137), and goat anti-HA (1:500, Novus Biologicals #NB600-362). Secondary antibodies raised in donkey and labeled with Alexa 488, Cy3, or Cy5 were used at 1:400 dilution (Jackson ImmunoResearch Laboratories).

Orthology analysis and phylogenetic inference

Accessions to all data used in orthology analysis are available in Table S2. We downloaded the predicted protein sequences of 65 nematode species and five outgroup taxa and filtered for the longest

535 isoform of each gene. OrthoFinder (Emms and Kelly, 2015) was used to cluster all protein sequences into
536 putative orthologous groups (OGs) using the default inflation value of 1.5. OGs containing loci which
537 were present in at least 75% of species and which were, on average, single copy (mean < 1.3) were
538 selected. We aligned each selected OG using MAFFT (Katoh and Standley, 2013) and generated a
539 maximum likelihood tree along with 1000 ultrafast bootstraps (Hoang et al., 2018) using IQ-TREE
540 (Nguyen et al., 2015), allowing the best-fitting substitution model to be selected automatically
541 (Kalyaanamoorthy et al., 2017). Each tree was screened by PhyloTreePruner (Kocot et al., 2013);
542 collapsing nodes with bootstrap support <90), and any OGs containing paralogues were discarded. If two
543 representative sequences were present for any species (*i.e.*, "in-paralogs") after this paralog screening
544 step, the longest of the two sequences was retained and the other discarded. We then realigned the
545 remaining OGs using MAFFT and trimmed spuriously aligned regions using trimAl (Capella-Gutiérrez et
546 al., 2009). The trimmed alignments were subsequently concatenated using catfasta2phyml (available at
547 https://github.com/nylander/catfasta2phyml) to form a supermatrix. We inferred the nematode species tree
548 using IQ-TREE with the general time reversible model (GTR) with gamma-distributed rate variation
549 among sites. The resulting tree was visualized using iTOL (Letunic and Bork, 2016).
550 We identified the OGs which contain orthologs of DMC-1, MND-1, HOP-2 and RAD-51 using
551 BLASTP to search using the orthologous protein sequences from *Homo sapiens* as queries. The OG
552 containing the *C. elegans* proteins HIM-8, ZIM-1, ZIM-2, ZIM-3 was identified using the appropriate
553 transcript IDs. Each OG was aligned using MAFFT and a gene tree was inferred using IQ-TREE,
554 allowing the best-fitting substitution model to be selected automatically. Each gene tree was visually
555 inspected using iTOL.
556
557 *Total RNAseq*
558 Total RNA was isolated from 20 whole worms or 30 dissected gonads from 48 h post J4 animals
559 using TRIzol (Invitrogen). TruSeq Stranded Total RNA (Illumina) sequencing libraries were constructed
560 following the manufacturer's instructions. For both conditions, three independent libraries were

561 constructed. Libraries were pooled and sequenced on a HiSeq4000 (150bp, PE, QB3 Vincent J. Coates
562 Genomics Sequencing Laboratory). Reads were mapped to the "El Paco" genome assembly including
563 annotated splice sites (Rödelsperger et al., 2017) using STAR. To correct misannotated splice sites, a
564 transcriptome was then reconstructed de novo using StringTie. Transdecoder was used to generate
565 potential open reading frames. To identify potential meiotic genes, we identified genes enriched in
566 dissected gonads over whole worms using HTSeq and edgeR.
567
568 **Acknowledgements**
569 This work was supported by funding from the Howard Hughes Medical Institute to AFD and a
570 fellowship from the Helen Hay Whitney Foundation to JB. This work used the Vincent J. Coates
571 Genomics Sequencing Laboratory at UC Berkeley, supported by NIH S10 OD018174 Instrumentation
572 Grant. We are grateful to Ralf J. Sommer, Ray Hong, and other members of the *P. pacificus* research
573 community for providing us with *P. pacificus* strains and abundant helpful advice. We thank members of
574 the Dernburg lab for helpful discussions about this work and critical reading of the manuscript.
575
576 **Figure Legends**
577 **Figure 1.** Germline organization and meiotic progression in *P. pacificus* is superficially similar to *C.*
578 *elegans*. A. Projection image of a *P. pacificus* hermaphrodite gonad stained with DAPI. Scale bar, 30
579 µm. Insets show representative nuclei from the premeiotic region (PM), transition zone (TZ), pachytene
580 (Pach), diplotene (Dip), diffuse stage (Diff) and diakinesis. Scale bar, 5 µm. B. Distal region of a *P.*
581 *pacificus* germline injected with 0.3 nM Cy3-dUTP solution, dissected and stained with DAPI after 30
582 minutes of recovery. Scale bar, 30 µm. C. Mitotic chromosomes (DAPI) in a 2-4 cell stage embryo and
583 the premeiotic germline of adult hermaphrodites expressing CENP-C::V5 (magenta). Scale bar, 2 µm.
584
585 **Figure 2.** Stable homolog pairing requires early recombination factors. A. Diagram showing the
586 locations of tandem repeat sequences used to generate DNA FISH probes for pairing analysis in *P.*

587 *pacificus*. B. Representative images show the progression of homolog pairing of Chromosome X
588 (magenta) and Chromosome IV (yellow) during meiotic prophase in wild-type hermaphrodites.
589 Premeiotic region (PM), transition zone (TZ), and pachytene (Pach). Scale bar, 5 μm. C. Representative
590 images of FISH probe signals in *spo-11*, *dmc-1*, and *rad-51* mutants during mid-prophase stage (roughly
591 equivalent to the pachytene stage in wild-type germlines). Scale bar, 5 μm. D. Temporal progression of X
592 and IV chromosome pairing in WT, *spo-11, dmc-1*, and *rad-51* mutants. Distance between pairs of
593 corresponding FISH signals were measured in 3D using Softworx or Prism for three gonads of each
594 genotype. Each gonad was divided into five zones of equal length, from the distal tip to the bend of the
595 gonad arm, and the distances between pairs of homologous FISH signals are presented in a scatter plot
596 diagram. E. Distance between pairs of heterologous FISH signals were measured in premeiotic (PM) and
597 transition zone (TZ) nuclei in WT, *spo-11* and *dmc-1* mutants (spanning zones 1 and 2 only). Distances
598 between pairs of homologous FISH signals (Chrom X and IV combined) in TZ nuclei are included for
599 comparison. ***p<.0001, by Student's *t*-test.
600
601 **Figure 2- Supplementary Figure 1.** Partial representation of the nematode lineage, including 65
602 nematode species, and five outgroup taxa showing the presence of meiotic proteins. D= Dmc1; M=
603 Mnd1; H= Hop2; Z= HIM-8/ZIM-1,2,3. *C. elegans* and *P. pacificus* are highlighted in blue.
604
605 **Figure 2- Supplementary Figure 2.** A. Composite projection images of whole gonads stained with
606 DAPI from WT, *spo-11*, *dmc-1*, and *rad-51* mutants. The extent of the transition zone of each gonad is
607 underlined with dashed lines. Scale bar, 30 μm. B. Quantification of transition zone length relative to the
608 length from meiotic onset to the end of pachytene in WT (n=7), *spo-11* (n=7), *dmc-1* (n=7), and *rad-51*
609 (n=10). Error bars indicate mean ± standard deviation. *spo-11* and *dmc-1* mutants show significant
610 differences from WT (p<0.0001) but not *Ppa-rad-51* (p=0.8426) by ordinary one-way ANOVA.
611

612 **Figure 3.** SPO-11 and DMC-1 are required, while RAD-51 is dispensable, for homologous synapsis in *P.*
613 *pacificus*. A. Composite projection image of a wild-type strain expressing Ppa-SYP-4::HA, stained with
614 DAPI (gray), anti-HOP-1 (red), and anti-HA (green). Meiotic progression is from left to right. Scale bar,
615 30 µm. B. Higher magnification images of wild-type nuclei in the premeiotic region (PM), transition
616 zone (TZ), pachytene (Pach), and pachy-diplotene (P-D) stages. C. Localization of Ppa-SYP-4::HA and
617 Ppa-HOP-1 in WT, *spo-11*, *dmc-1*, and *rad-51* mutants during early and mid-prophase (roughly
618 equivalent to the TZ and Pach regions in wild-type germlines, respectively). Synapsis fails in *spo-11* and
619 *dmc-1* mutants but forms normally in the *rad-51* background. Scale bar, 5 µm.
620
621 **Figure 4.** DMC-1 and RAD-51 localize sequentially to meiotic chromosomes. A. Composite projection
622 image of a wild-type gonad expressing DMC-1::V5, stained with DAPI (blue), anti-V5 (magenta), and
623 anti-RAD-51 (yellow). Meiotic progression is from left to right. Scale bar, 30 µm. Inset shows the distinct
624 localization of DMC-1 (magenta) and RAD-51 (yellow) in the transition zone and pachytene regions,
625 respectively. Scale bar, 5 µm. B. Higher magnification images of nuclei in the transition zone and
626 pachytene region. DMC-1 is present along chromatin in the transition zone and disappears at pachytene.
627 By contrast, RAD-51 localizes to discrete foci starting at pachytene. Scale bar, 5 µm. C. Occasional
628 nucleus on the border of the transition zone and pachytene region display both DMC-1 and RAD-51. The
629 signals do not completely overlap. Scale bar, 2 µm. D. Nucleus with clustered DAPI morphology and
630 strong association of DMC-1 during later prophase. DMC-1 localizes to chromatin in "straggler" cells
631 that presumably have not completed synapsis or CO designation, or are undergoing apoptosis. Scale bar,
632 2 µm.
633
634 **Figure 4- Supplementary Figure 1.** DMC-1 and RAD-51 do not depend on each other for their
635 localization to chromosomes, but both require DSBs. A. DMC-1 (magenta) is abundant on chromosomes
636 in transition zone nuclei of *rad-51* mutants. Anti-RAD-51 immunofluorescence was used to identify
637 homozygous mutants among the progeny of heterozygotes. B. RAD-51 foci are observed in late

638 pachytene nuclei, proximal to the extended transition zone, of *dmc-1* mutants. RAD-51 foci appear larger
639 and more numerous than in wild-type pachytene nuclei. C. DMC-1 forms nuclear aggregates in *spo-11*
640 mutants and does not localize along chromosomes. D and E. RAD-51 foci are detected in premeiotic
641 nuclei of *spo-11* mutants but are absent during meiotic prophase.
642
643 **Figure 5.** Crossover formation requires SPO-11 and DMC-1, but not RAD-51. A. Representative images
644 of DAPI-staining bodies at diakinesis for each indicated genotype. Scale bar, 5 µm. B. Quantification of
645 DAPI-staining bodies in the -1 oocyte at diakinesis for each indicated genotype (*n*= represents number of
646 nuclei scored). C. Quantification of gonads which lacked nuclei with DAPI-staining bodies at diakinesis
647 stage. *n* is the number of germlines scored for each genotype. D. Representative images of wild type,
648 *dmc-1*, and *rad-51* mutant proximal germlines. In wild-type germlines, diakinesis nuclei with fully
649 condensed DAPI-staining bodies are present distal to the spermatheca. However, nuclei with late
650 prophase stage DAPI morphology are frequently found adjacent to the spermatheca in *dmc-1* mutants and
651 more rarely in *rad-51* mutants. Meiotic progression is from left to right. Scale bar, 5 µm. E. Frequencies
652 of viable embryos and male progeny of whole broods from wild type, *spo-11*, *dmc-1* and *rad-51* mutant
653 hermaphrodites.
654
655 **Figure 6.** COSA-1/Cntd1 accumulates at a single site per chromosome pair. A. Composite projection
656 image of a wild-type strain expressing three epitope-tagged proteins (COSA-1::3xFLAG, DMC-1::V5,
657 and SYP-4::HA), stained with anti-FLAG, anti-V5 and anti-HA antibodies. Scale bar, 30 µm. B. Higher
658 magnification images of nuclei from the transition zone (TZ), pachytene (pach), mid- and late pachy-
659 diplotene (P-D). COSA-1::3xFLAG (green) foci are detected in transition zone nuclei but do not
660 colocalize with DMC-1::V5 (cyan). Foci peak in brightness in pachytene nuclei and gradually become
661 dimmer until they are no longer detected during late pachy-diplotene. In early to mid- pachy-diplotene
662 nuclei, six short stretches of SYP-4::HA (magenta) are observed per nucleus, each associated with a
663 single COSA-1::3xFLAG focus. Scale bar, 5 µm. C. Histogram showing the number of COSA-

664 1::3xFLAG foci observed per nucleus in the pachytene region. Analysis was restricted to 15 nuclei per
665 gonad immediately proximal to the transition zone and lacking DMC-1::V5 signal. Five individual
666 gonads were analyzed, for a total of 75 nuclei scored. D. Partial projection of a representative nucleus in
667 mid to late pachy-diplotene, stained with anti-HOP-1 (blue), anti-HA (marking the SC, magenta), and
668 anti-FLAG (marking COSA-1, green). A single COSA-1::3xFLAG focus is observed at a junction
669 (marked with a red arrowhead) between the "short arm," where SYP-4::HA is retained, and splayed "long
670 arms" lacking SC but positive for HOP-1. Scale bar, 2 μm.
671
672 **Figure 6 - Supplemental Figure 1.** COSA-1/Cntd1 accumulates at a single site per chromosome pair
673 during spermatogenesis. Composite projection image of a wild-type gonad from a J4-stage hermaphrodite
674 expressing COSA-1::3xFLAG (green) and SYP-4::HA (magenta). Scale bar, 30 μm. At this stage the
675 germline is still undergoing spermatogenesis. Inset shows a higher magnification image of nuclei in the
676 pachytene region. As during oogenesis, ~6 COSA-1::3xFLAG foci are observed in pachytene nuclei
677 during spermatogenesis. Scale bar, 5 μm.
678
679 **Figure 6 - Supplementary Video 1.** COSA-1/Cntd1 accumulates at a single site per chromosome pair.
680 3D volume rendering of a single nucleus from the pachytene region of a wild-type worm expressing
681 COSA-1::3xFLAG (green) and SYP-4::HA (magenta). Each frame is a maximum intensity projection
682 from a region of a deconvolved 3D image. Each stretch of SYP-4::HA is associated with a COSA-
683 1::3xFLAG focus.
684
685 **Figure 7.** COSA-1::3xFLAG accumulates at sites of presumptive Class I COs. A. Nuclei from
686 hermaphrodites of the indicated genotype displaying COSA-1::3xFLAG (green) in early and mid-
687 prophase (roughly equivalent to the transition zone and pachytene regions in wild-type germlines,
688 respectively). COSA-1 foci are absent in *dmc-1* mutants, but 6 foci per nucleus are detected in wild type
689 and *rad-51* mutants. A few small foci are detected in s*po-11* mutants. Scale bar, 5 μm.

690

691

692 **REFERENCES**

693 Aravind L, Koonin EV. 1998. The HORMA domain: a common structural denominator in mitotic
694 checkpoints, chromosome synapsis and DNA repair. *Trends Biochem Sci* **23**:284–286.
695 Benson G. 1999. Tandem repeats finder: a program to analyze DNA sequences. *Nucleic Acids Research*.
696 doi:10.1093/nar/27.2.573
697 Bishop DK, Park D, Xu L, Kleckner N. 1992. DMC1: A meiosis-specific yeast homolog of E. coli recA
698 required for recombination, synaptonemal complex formation, and cell cycle progression. *Cell*
699 **69**:439–456. doi:10.1016/0092-8674(92)90446-j
700 Bolt BJ, Rodgers FH, Shafie M, Kersey PJ, Berriman M, Howe KL. 2018. Using WormBase ParaSite: An
701 Integrated Platform for Exploring Helminth Genomic Data. *Methods Mol Biol* **1757**:471–491.
702 doi:10.1007/978-1-4939-7737-6_15
703 Brenner S. 1974. The genetics of Caenorhabditis elegans. *Genetics* **77**:71–94.
704 Capella-Gutiérrez S, Silla-Martínez JM, Gabaldón T. 2009. trimAl: a tool for automated alignment
705 trimming in large-scale phylogenetic analyses. *Bioinformatics* **25**:1972–1973.
706 doi:10.1093/bioinformatics/btp348
707 Christophorou N, Rubin T, Huynh J-R. 2013. Synaptonemal complex components promote centromere
708 pairing in pre-meiotic germ cells. *PLoS Genet* **9**:e1004012. doi:10.1371/journal.pgen.1004012
709 Cloud V, Chan Y-L, Grubb J, Budke B, Bishop DK. 2012. Rad51 is an accessory factor for Dmc1-
710 mediated joint molecule formation during meiosis. *Science* **337**:1222–1225.
711 doi:10.1126/science.1219379
712 Colaiácovo MP, MacQueen AJ, Martinez-Perez E, McDonald K, Adamo A, La Volpe A, Villeneuve AM.
713 2003. Synaptonemal Complex Assembly in C. elegans Is Dispensable for Loading Strand-Exchange
714 Proteins but Critical for Proper Completion of Recombination. *Developmental Cell*.
715 doi:10.1016/s1534-5807(03)00232-6
716 Couteau F, Belzile F, Horlow C, Grandjean O, Vezon D, Doutriaux M-P. 1999. Random Chromosome
717 Segregation without Meiotic Arrest in Both Male and Female Meiocytes of a dmc1 Mutant of
718 Arabidopsis. *Plant Cell* **11**:1623. doi:10.2307/3871042
719 Da Ines O, Degroote F, Goubely C, Amiard S, Gallego ME, White CI. 2013. Meiotic Recombination in
720 Arabidopsis Is Catalysed by DMC1, with RAD51 Playing a Supporting Role. *PLoS Genet*
721 **9**:e1003787. doi:10.1371/journal.pgen.1003787
722 Dieterich C, Clifton SW, Schuster LN, Chinwalla A, Delehaunty K, Dinkelacker I, Fulton L, Fulton R,
723 Godfrey J, Minx P, Mitreva M, Roeseler W, Tian H, Witte H, Yang S-P, Wilson RK, Sommer RJ.
724 2008. The Pristionchus pacificus genome provides a unique perspective on nematode lifestyle and
725 parasitism. *Nat Genet* **40**:1193–1198. doi:10.1038/ng.227
726 Emms DM, Kelly S. 2015. OrthoFinder: solving fundamental biases in whole genome comparisons
727 dramatically improves orthogroup inference accuracy. *Genome Biol* **16**:157. doi:10.1186/s13059-
728 015-0721-2
729 Enguita-Marruedo A, Martín-Ruiz M, García E, Gil-Fernández A, Parra MT, Viera A, Rufas JS, Page J.
730 2019. Transition from a meiotic to a somatic-like DNA damage response during the pachytene stage
731 in mouse meiosis. *PLoS Genet* **15**:e1007439. doi:10.1371/journal.pgen.1007439
732 Gray S, Cohen PE. 2016. Control of Meiotic Crossovers: From Double-Strand Break Formation to
733 Designation. *Annu Rev Genet* **50**:175–210. doi:10.1146/annurev-genet-120215-035111
734 Grelon M. 2001. AtSPO11-1 is necessary for efficient meiotic recombination in plants. *EMBO J* **20**:589–
735 600. doi:10.1093/emboj/20.3.589
736 Harper NC, Rillo R, Jover-Gil S, Assaf ZJ, Bhalla N, Dernburg AF. 2011. Pairing centers recruit a Polo-

like kinase to orchestrate meiotic chromosome dynamics in C. elegans. *Dev Cell* **21**:934–947. doi:10.1016/j.devcel.2011.09.001

Hayashi M, Chin GM, Villeneuve AM. 2007. C. elegans germ cells switch between distinct modes of double-strand break repair during meiotic prophase progression. *PLoS Genet* **3**:e191. doi:10.1371/journal.pgen.0030191

Hillers KJ, Jantsch V, Martinez-Perez E, Yanowitz JL. 2017. Meiosis. *WormBook* **2017**:1–43. doi:10.1895/wormbook.1.178.1

Hoang DT, Chernomor O, von Haeseler A, Minh BQ, Vinh LS. 2018. UFBoot2: Improving the Ultrafast Bootstrap Approximation. *Mol Biol Evol* **35**:518–522. doi:10.1093/molbev/msx281

Hong EL, Shinohara A, Bishop DK. 2001. Saccharomyces cerevisiae Dmc1 protein promotes renaturation of single-strand DNA (ssDNA) and assimilation of ssDNA into homologous super-coiled duplex DNA. *J Biol Chem* **276**:41906–41912. doi:10.1074/jbc.M105563200

Hong RL, Sommer RJ. 2006. Pristionchus pacificus: a well-rounded nematode. *Bioessays* **28**:651–659. doi:10.1002/bies.20404

Joyce EF, Apostolopoulos N, Beliveau BJ, Wu C-T. 2013. Germline progenitors escape the widespread phenomenon of homolog pairing during Drosophila development. *PLoS Genet* **9**:e1004013. doi:10.1371/journal.pgen.1004013

Kalyaanamoorthy S, Minh BQ, Wong TKF, von Haeseler A, Jermiin LS. 2017. ModelFinder: fast model selection for accurate phylogenetic estimates. *Nat Methods* **14**:587–589. doi:10.1038/nmeth.4285

Katoh K, Standley DM. 2013. MAFFT multiple sequence alignment software version 7: improvements in performance and usability. *Mol Biol Evol* **30**:772–780. doi:10.1093/molbev/mst010

Keeney S. 2008. Spo11 and the Formation of DNA Double-Strand Breaks in Meiosis. *Genome Dyn Stab* **2**:81–123. doi:10.1007/7050_2007_026

Keeney S, Giroux CN, Kleckner N. 1997. Meiosis-specific DNA double-strand breaks are catalyzed by Spo11, a member of a widely conserved protein family. *Cell* **88**:375–384.

Kim Y, Kostow N, Dernburg AF. 2015. The Chromosome Axis Mediates Feedback Control of CHK-2 to Ensure Crossover Formation in C. elegans. *Dev Cell* **35**:247–261. doi:10.1016/j.devcel.2015.09.021

Kocot KM, Citarella MR, Moroz LL, Halanych KM. 2013. PhyloTreePruner: A Phylogenetic Tree-Based Approach for Selection of Orthologous Sequences for Phylogenomics. *Evol Bioinform Online* **9**:429–435. doi:10.4137/EBO.S12813

Labella S, Woglar A, Jantsch V, Zetka M. 2011. Polo kinases establish links between meiotic chromosomes and cytoskeletal forces essential for homolog pairing. *Dev Cell* **21**:948–958. doi:10.1016/j.devcel.2011.07.011

Letunic I, Bork P. 2016. Interactive tree of life (iTOL) v3: an online tool for the display and annotation of phylogenetic and other trees. *Nucleic Acids Res* **44**:W242–5. doi:10.1093/nar/gkw290

Li Z, Golub EI, Gupta R, Radding CM. 1997. Recombination activities of HsDmc1 protein, the meiotic human homolog of RecA protein. *Proc Natl Acad Sci U S A* **94**:11221–11226.

Lo T-W, Pickle CS, Lin S, Ralston EJ, Gurling M, Schartner CM, Bian Q, Doudna JA, Meyer BJ. 2013. Precise and heritable genome editing in evolutionarily diverse nematodes using TALENs and CRISPR/Cas9 to engineer insertions and deletions. *Genetics* **195**:331–348. doi:10.1534/genetics.113.155382

Lui DY, Colaiácovo MP. 2012. Meiotic Development in Caenorhabditis elegansAdvances in Experimental Medicine and Biology. pp. 133–170. doi:10.1007/978-1-4614-4015-4_6

MacQueen AJ, Colaiácovo MP, McDonald K, Villeneuve AM. 2002. Synapsis-dependent and -independent mechanisms stabilize homolog pairing during meiotic prophase in C. elegans. *Genes Dev* **16**:2428–2442. doi:10.1101/gad.1011602

MacQueen AJ, Phillips CM, Bhalla N, Weiser P, Villeneuve AM, Dernburg AF. 2005. Chromosome sites play dual roles to establish homologous synapsis during meiosis in C. elegans. *Cell* **123**:1037–1050. doi:10.1016/j.cell.2005.09.034

Martinez-Perez E, Colaiácovo MP. 2009. Distribution of meiotic recombination events: talking to your neighbors. *Curr Opin Genet Dev* **19**:105–112. doi:10.1016/j.gde.2009.02.005

Martin JS, Winkelmann N, Petalcorin MIR, McIlwraith MJ, Boulton SJ. 2005. RAD-51-dependent and -independent roles of a Caenorhabditis elegans BRCA2-related protein during DNA double-strand break repair. *Mol Cell Biol* **25**:3127–3139. doi:10.1128/MCB.25.8.3127-3139.2005

Masson JY, Davies AA, Hajibagheri N, Van Dyck E, Benson FE, Stasiak AZ, Stasiak A, West SC. 1999. The meiosis-specific recombinase hDmc1 forms ring structures and interacts with hRad51. *EMBO J* **18**:6552–6560. doi:10.1093/emboj/18.22.6552

Nadarajan S, Lambert TJ, Altendorfer E, Gao J, Blower MD, Waters JC, Colaiácovo MP. 2017. Polo-like kinase-dependent phosphorylation of the synaptonemal complex protein SYP-4 regulates double-strand break formation through a negative feedback loop. *Elife* **6**. doi:10.7554/eLife.23437

Namai S, Sugimoto A. 2018. Transgenesis by microparticle bombardment for live imaging of fluorescent proteins in Pristionchus pacificus germline and early embryos. *Dev Genes Evol* **228**:75–82. doi:10.1007/s00427-018-0605-z

Nguyen L-T, Schmidt HA, von Haeseler A, Minh BQ. 2015. IQ-TREE: a fast and effective stochastic algorithm for estimating maximum-likelihood phylogenies. *Mol Biol Evol* **32**:268–274. doi:10.1093/molbev/msu300

Pattabiraman D, Roelens B, Woglar A, Villeneuve AM. 2017. Meiotic recombination modulates the structure and dynamics of the synaptonemal complex during C. elegans meiosis. doi:10.1101/110064

Penkner AM, Fridkin A, Gloggnitzer J, Baudrimont A, Machacek T, Woglar A, Csaszar E, Pasierbek P, Ammerer G, Gruenbaum Y, Jantsch V. 2009. Meiotic chromosome homology search involves modifications of the nuclear envelope protein Matefin/SUN-1. *Cell* **139**:920–933. doi:10.1016/j.cell.2009.10.045

Phillips CM, Dernburg AF. 2006. A family of zinc-finger proteins is required for chromosome-specific pairing and synapsis during meiosis in C. elegans. *Dev Cell* **11**:817–829. doi:10.1016/j.devcel.2006.09.020

Phillips CM, Wong C, Bhalla N, Carlton PM, Weiser P, Meneely PM, Dernburg AF. 2005. HIM-8 binds to the X chromosome pairing center and mediates chromosome-specific meiotic synapsis. *Cell* **123**:1051–1063. doi:10.1016/j.cell.2005.09.035

Pires-daSilva A. 2004. Conservation of the global sex determination gene tra-1 in distantly related nematodes. *Genes Dev* **18**:1198–1208. doi:10.1101/gad.293504

Pittman DL, Cobb J, Schimenti KJ, Wilson LA, Cooper DM, Brignull E, Handel MA, Schimenti JC. 1998. Meiotic Prophase Arrest with Failure of Chromosome Synapsis in Mice Deficient for Dmc1 , a Germline-Specific RecA Homolog. *Mol Cell* **1**:697–705. doi:10.1016/s1097-2765(00)80069-6

Rinaldo C, Bazzicalupo P, Ederle S, Hilliard M, La Volpe A. 2002. Roles for Caenorhabditis elegans rad-51 in meiosis and in resistance to ionizing radiation during development. *Genetics* **160**:471–479.

Rockmill B, Sym M, Scherthan H, Roeder GS. 1995. Roles for two RecA homologs in promoting meiotic chromosome synapsis. *Genes Dev* **9**:2684–2695. doi:10.1101/gad.9.21.2684

Rödelsperger C, Meyer JM, Prabh N, Lanz C, Bemm F, Sommer RJ. 2017. Single-Molecule Sequencing Reveals the Chromosome-Scale Genomic Architecture of the Nematode Model Organism Pristionchus pacificus. *Cell Rep* **21**:834–844. doi:10.1016/j.celrep.2017.09.077

Rog O, Dernburg AF. 2013. Chromosome pairing and synapsis during Caenorhabditis elegans meiosis. *Current Opinion in Cell Biology*. doi:10.1016/j.ceb.2013.03.003

Rubin T, Christophorou N, Huynh J-R. 2016. How to pre-pair chromosomes for meiosis. *Cell Cycle* **15**:609–610. doi:10.1080/15384101.2015.1131524

Rudel D, Riebesell M, Sommer RJ. 2005. Gonadogenesis in Pristionchus pacificus and organ evolution: development, adult morphology and cell–cell interactions in the hermaphrodite gonad. *Developmental Biology*. doi:10.1016/j.ydbio.2004.09.021

Sato A, Isaac B, Phillips CM, Rillo R, Carlton PM, Wynne DJ, Kasad RA, Dernburg AF. 2009. Cytoskeletal forces span the nuclear envelope to coordinate meiotic chromosome pairing and synapsis. *Cell* **139**:907–919. doi:10.1016/j.cell.2009.10.039

Smolikov S, Eizinger A, Schild-Prufert K, Hurlburt A, McDonald K, Engebrecht J, Villeneuve AM, Colaiácovo MP. 2007. SYP-3 restricts synaptonemal complex assembly to bridge paired

chromosome axes during meiosis in Caenorhabditis elegans. *Genetics* **176**:2015–2025. doi:10.1534/genetics.107.072413

Smolikov S, Schild-Prüfert K, Colaiácovo MP. 2009. A yeast two-hybrid screen for SYP-3 interactors identifies SYP-4, a component required for synaptonemal complex assembly and chiasma formation in Caenorhabditis elegans meiosis. *PLoS Genet* **5**:e1000669. doi:10.1371/journal.pgen.1000669

Sommer RJ. 2015. Pristionchus pacificus: A Nematode Model for Comparative and Evolutionary Biology. BRILL.

Sommer RJ, Carta LK, Kim S-Y, Sternburg PW. 1996. Morphological, genetic and molecular description of Pristionchus pacificus sp. N. (Nematoda: Neodiplogastridae). *Fundam. Appl. Nematol.* **19:** 511-521

Srinivasan J, Sinz W, Jesse T, Wiggers-Perebolte L, Jansen K, Buntjer J, van der Meulen M, Sommer RJ. 2003. An integrated physical and genetic map of the nematode Pristionchus pacificus. *Mol Genet Genomics* **269**:715–722. doi:10.1007/s00438-003-0881-8

Srinivasan J, Sinz W, Lanz C, Brand A, Nandakumar R, Raddatz G, Witte H, Keller H, Kipping I, Pires-daSilva A, Jesse T, Millare J, de Both M, Schuster SC, Sommer RJ. 2002. A bacterial artificial chromosome-based genetic linkage map of the nematode Pristionchus pacificus. *Genetics* **162**:129–134.

Vader G, Musacchio A. 2014. HORMA domains at the heart of meiotic chromosome dynamics. *Dev Cell* **31**:389–391. doi:10.1016/j.devcel.2014.11.009

Villeneuve AM, Hillers KJ. 2001. Whence meiosis? *Cell* **106**:647–650.

Witte H, Moreno E, Rödelsperger C, Kim J, Kim J-S, Streit A, Sommer RJ. 2015. Gene inactivation using the CRISPR/Cas9 system in the nematode Pristionchus pacificus. *Dev Genes Evol* **225**:55–62. doi:10.1007/s00427-014-0486-8

Yokoo R, Zawadzki KA, Nabeshima K, Drake M, Arur S, Villeneuve AM. 2012. COSA-1 reveals robust homeostasis and separable licensing and reinforcement steps governing meiotic crossovers. *Cell* **149**:75–87. doi:10.1016/j.cell.2012.01.052

Yoshida K, Kondoh G, Matsuda Y, Habu T, Nishimune Y, Morita T. 1998. The Mouse RecA -like Gene Dmc1 Is Required for Homologous Chromosome Synapsis during Meiosis. *Mol Cell* **1**:707–718. doi:10.1016/s1097-2765(00)80070-2

Zickler D, Kleckner N. 1999. Meiotic chromosomes: integrating structure and function. *Annu Rev Genet* **33**:603–754. doi:10.1146/annurev.genet.33.1.603

Figure 1

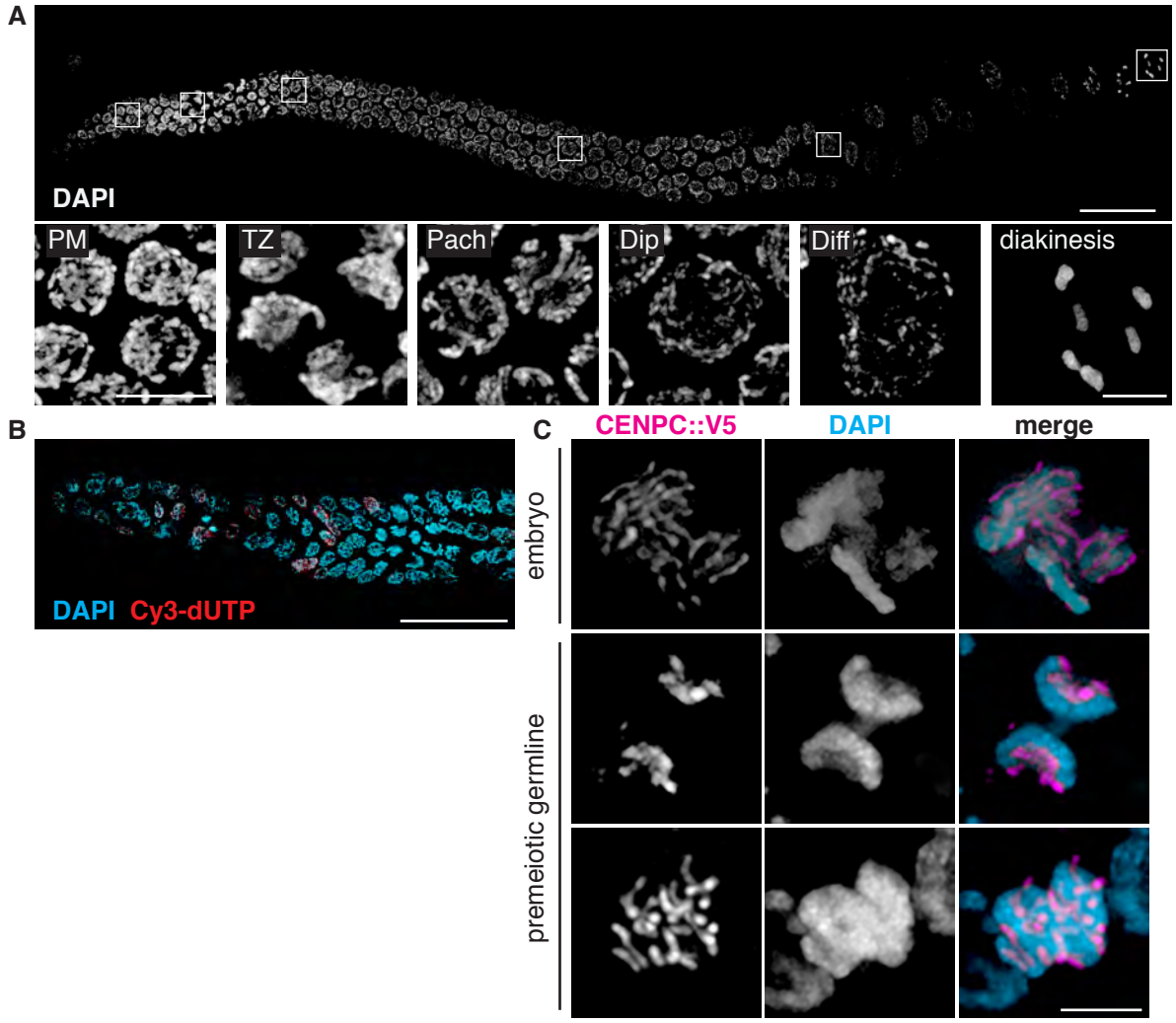

Figure 2

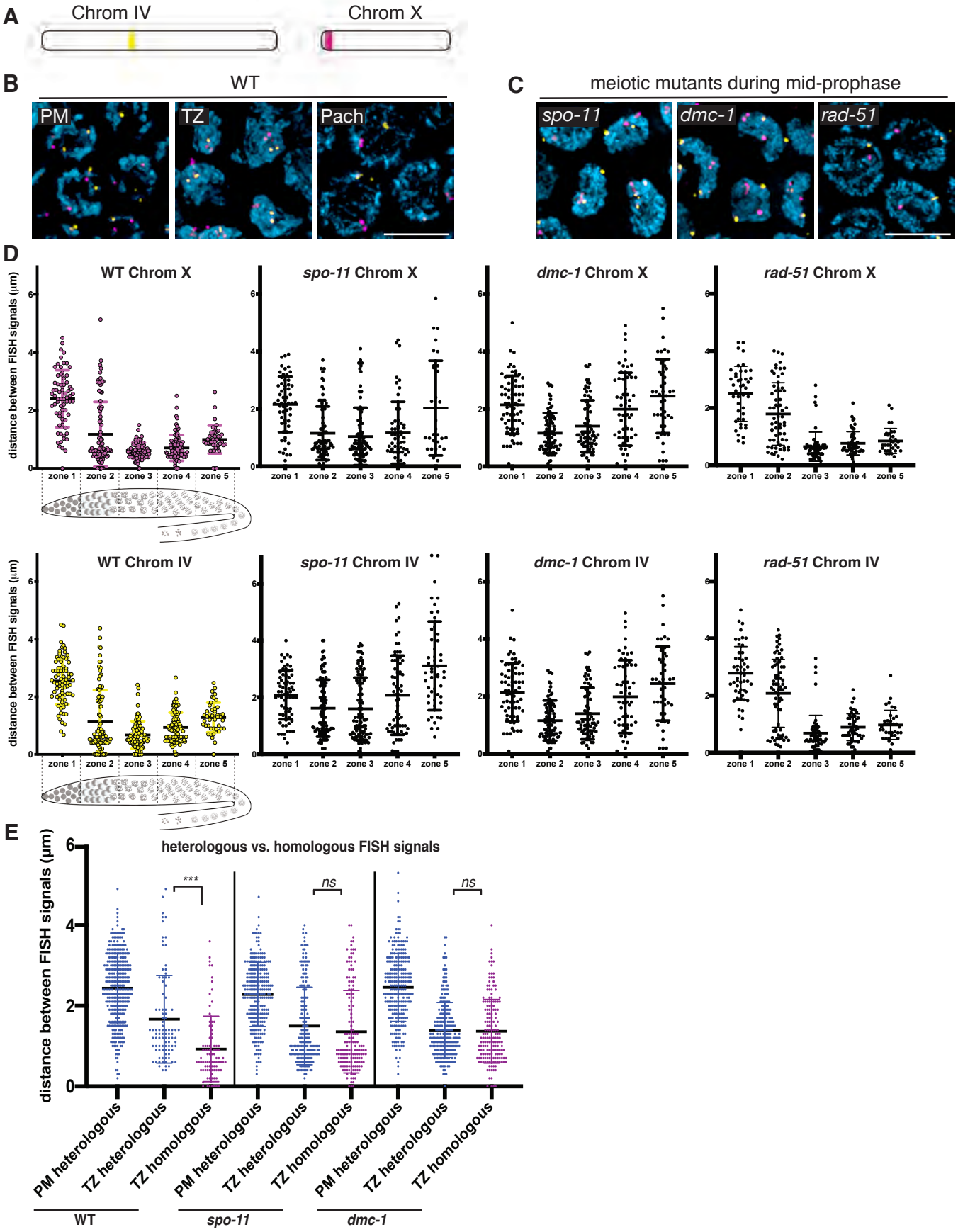

Figure 2- figure supplement 1

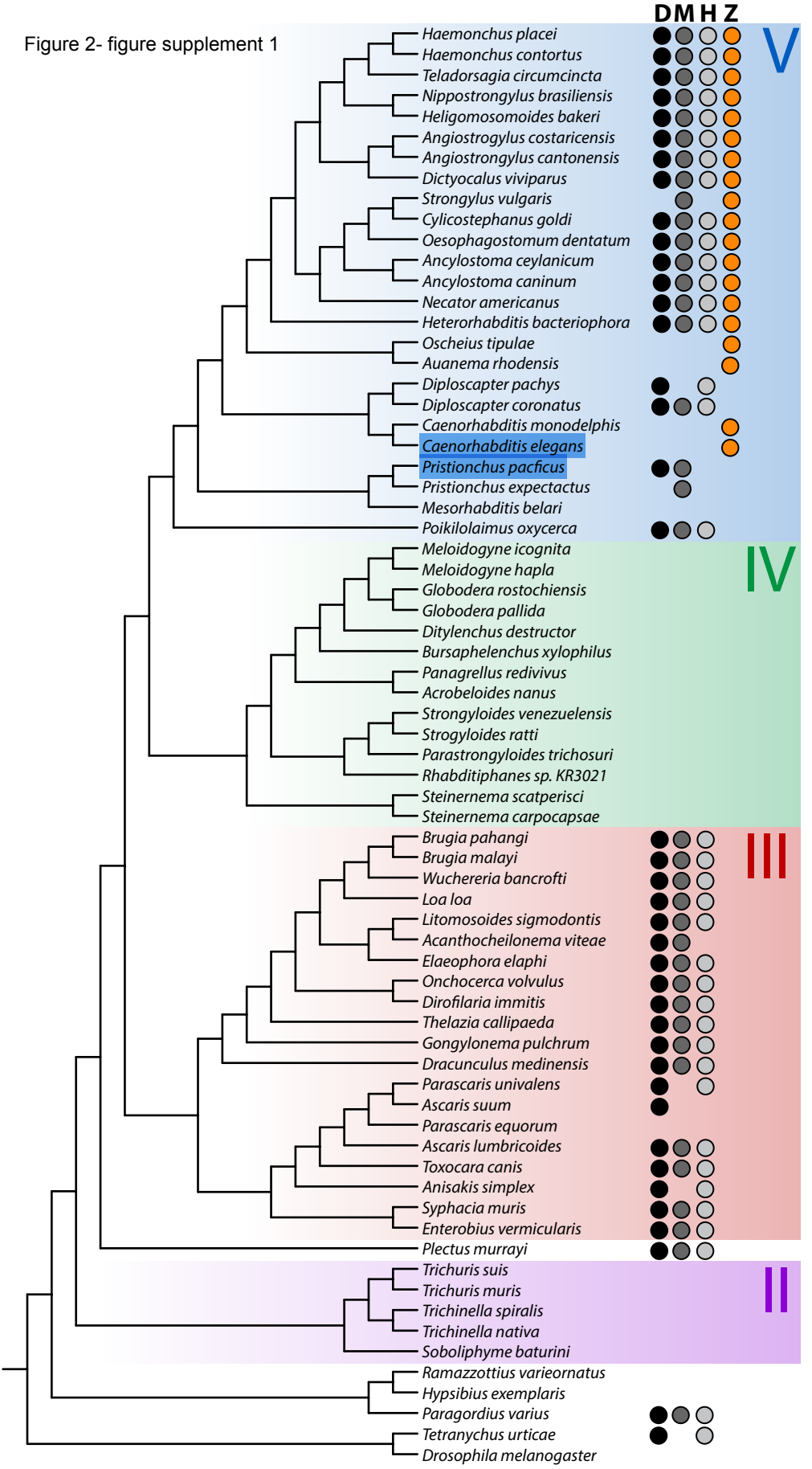

Figure 2- figure supplement 2

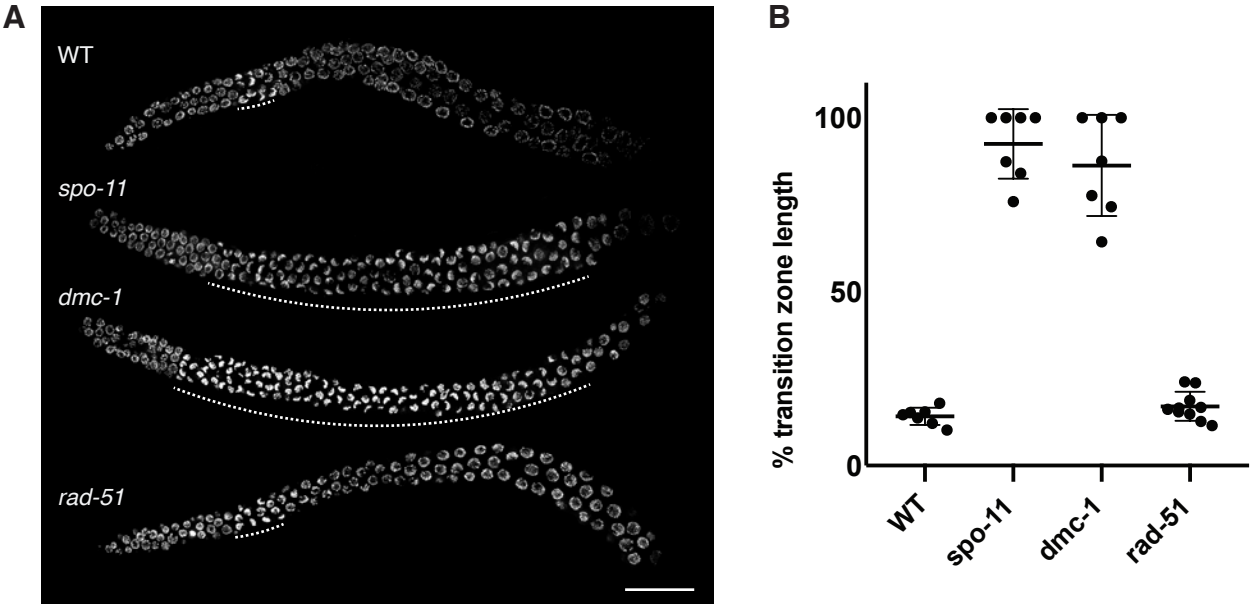

Figure 3

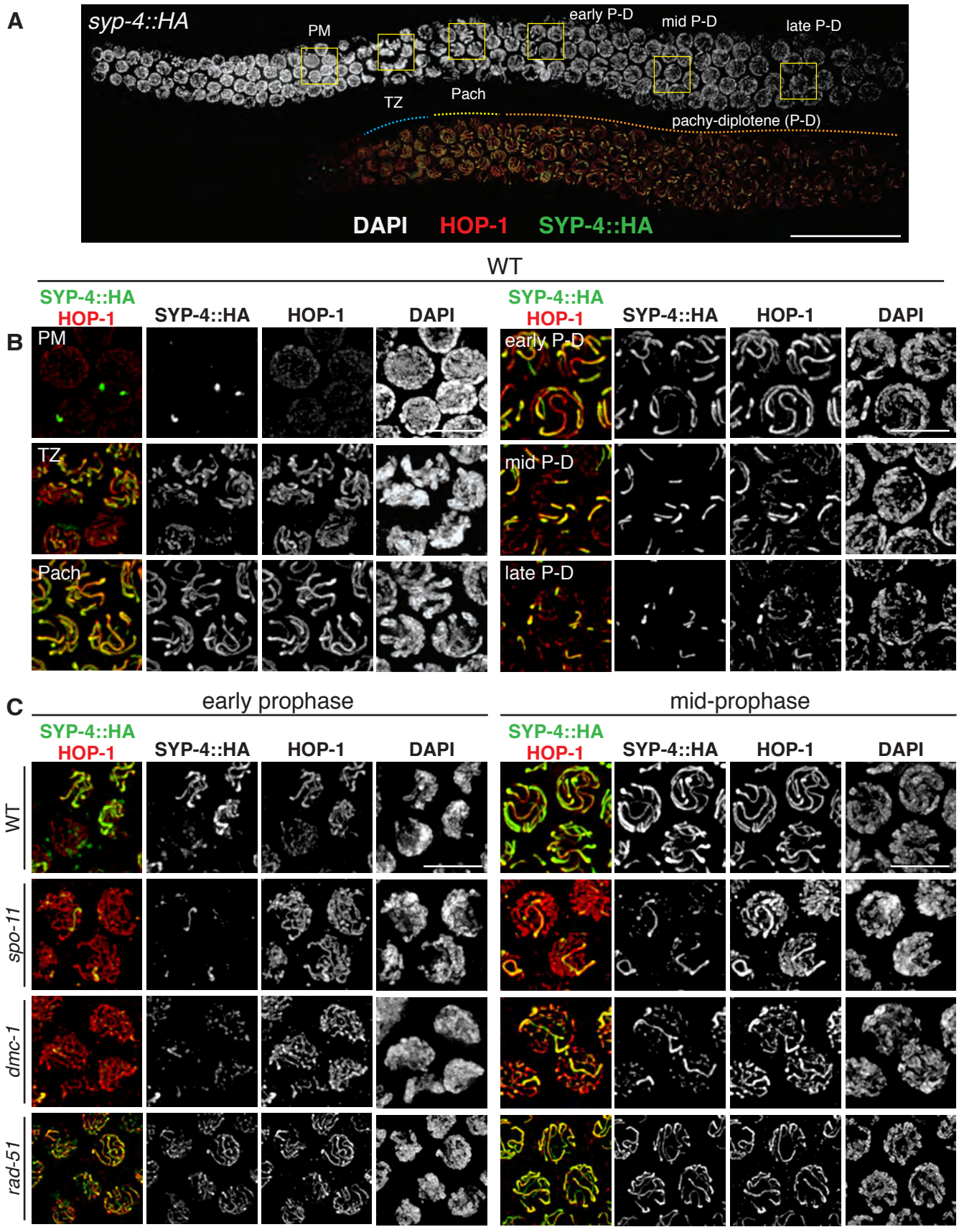

Figure 3- figure supplement 1

Genotype	% Egg viability (±SD)	% Male progeny (±SD)	Eggs laid (± SD)
WT (n=30)	92.9 (±16.3)	0.9 (±1.0)	205 (±55)
syp-4::HA (n=7)	97.7 (±11.0)	.5 (±0.6)	164 (±15)
dmc-1::V5 (n=8)	95.3 (±4.7)	1.1 (±1.4)	170 (±14)
syp-4::HA; dmc-1::V5; cosa-1::3xFLAG (n=8)	87.0 (±10.6)	.4 (±0.6)	170 (±37)

Figure 4

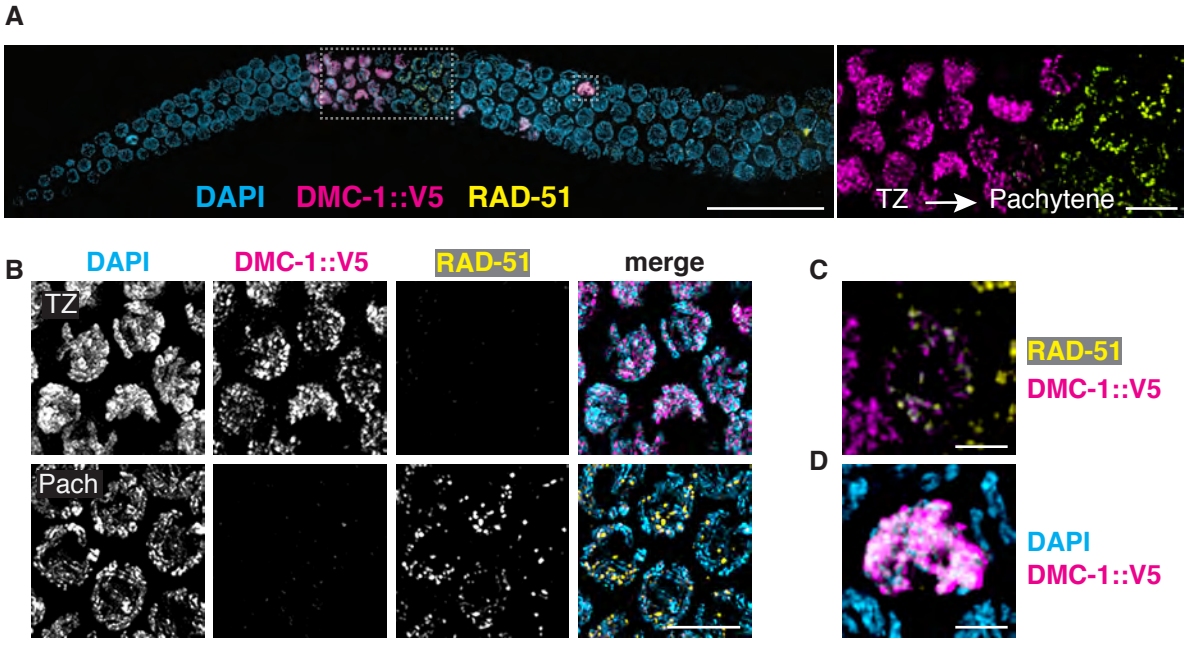

Figure 4- figure supplement 1

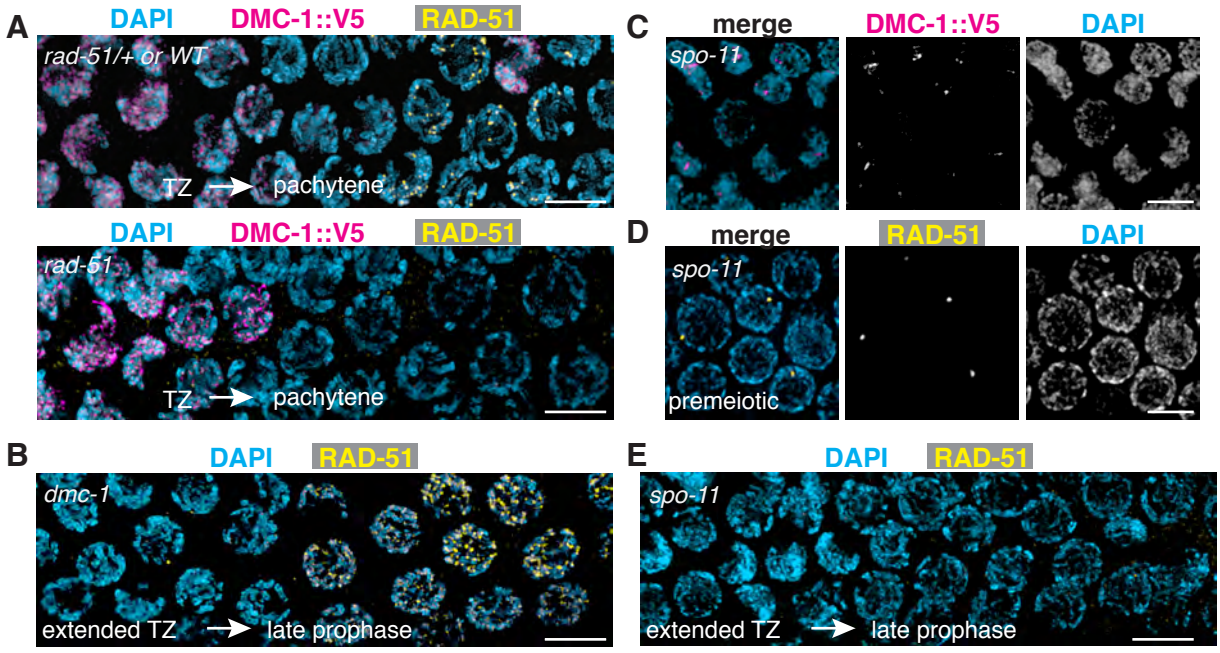

Figure 5

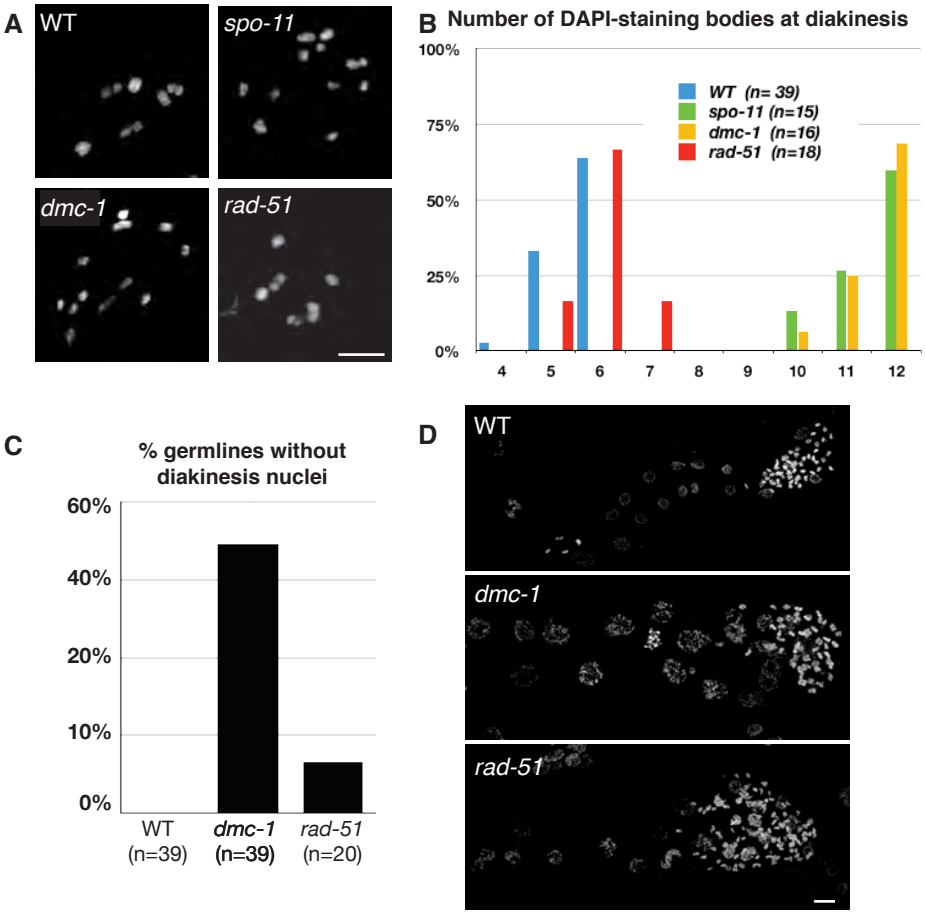

E

Genotype	% Egg viability (±SD)	% Male progeny (±SD)	Eggs laid (± SD)
WT (n=30)	92.9 (±16.3)	0.9 (±1.0)	205 (±55)
spo-11 (n=5)	0.3 (± .4)	20 (±44.7)	125 (±40)
dmc-1 (n=7)	0 (±0)	N/A	12 (±12)
rad-51 (n=14)	15.0 (±17.9)	4.5 (±5.1)	121 (±70)

Figure 6

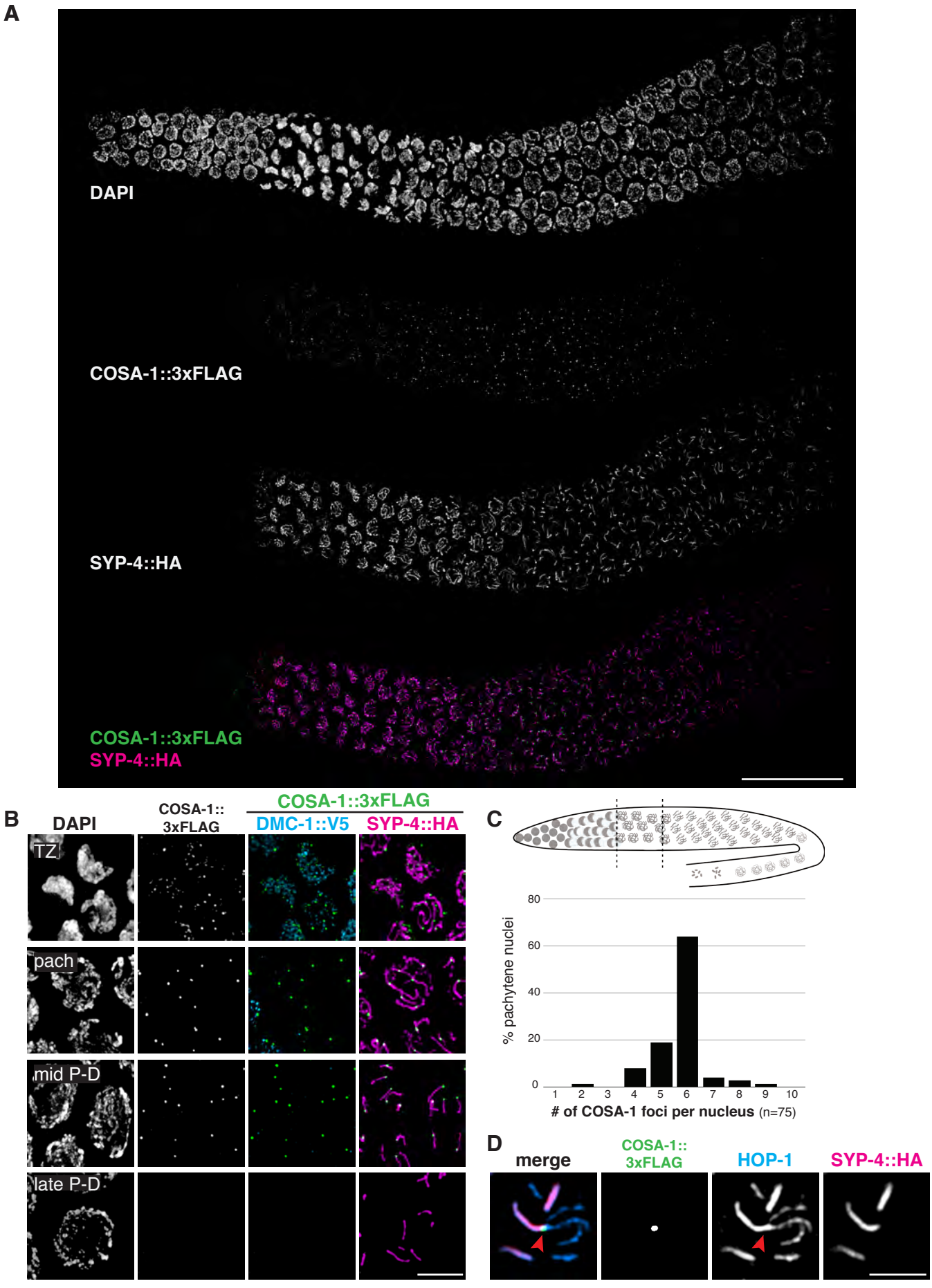

Figure 6- figure supplement 1

A

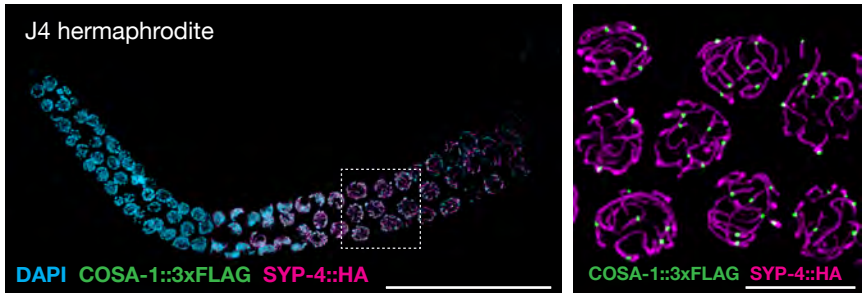

Figure 7

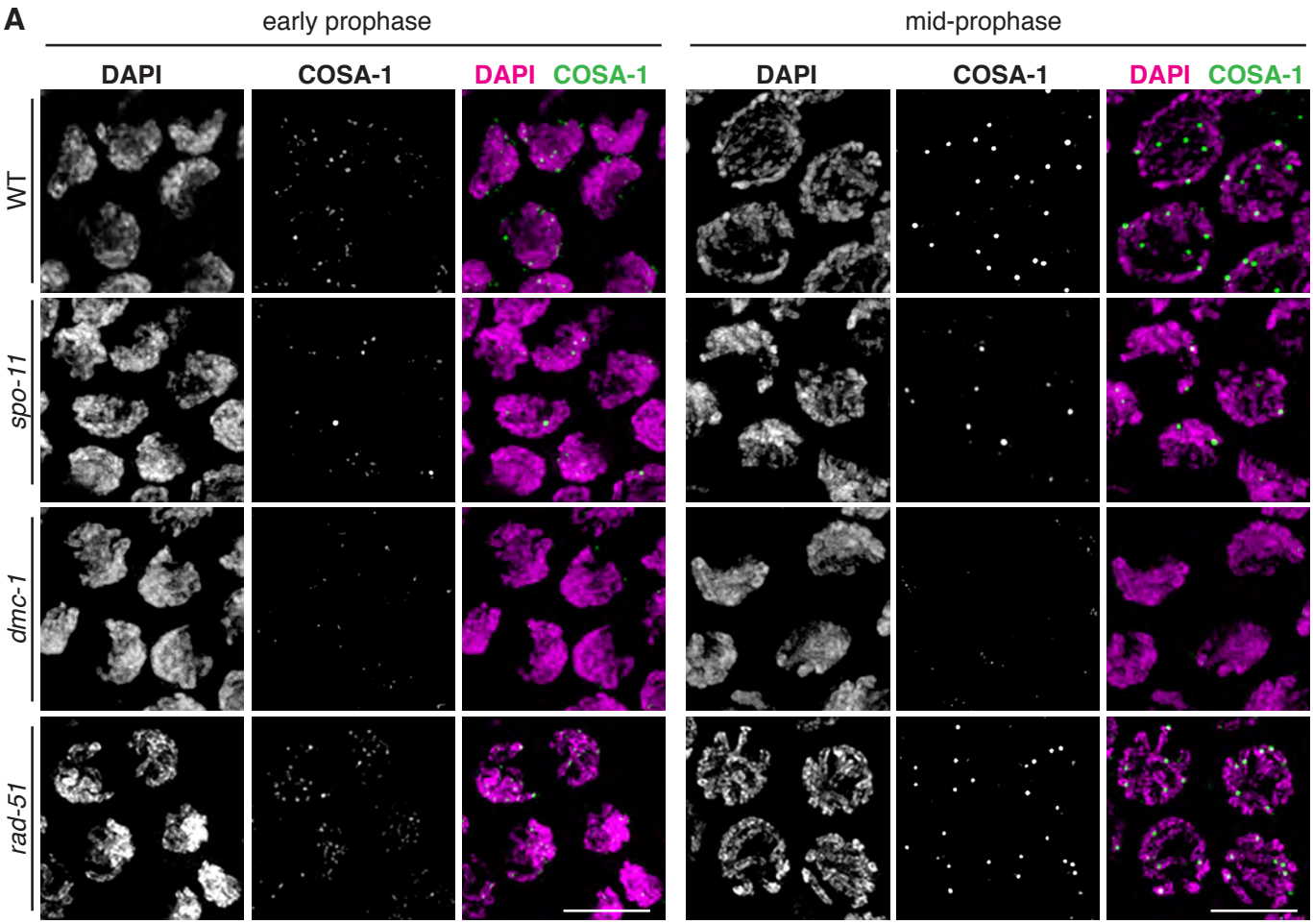

Table S1

Strain	El Paco genome reference, v1, 2017	Wormbase designation	Allele	guide RNA target sequence (PAM sequence underlined)	ssDNA template	genotyping primer sequences
cenpc::V5	*UMM-S71-6.7-mRNA-1*	*PPA37734*	*ie1007*	ATGAAGAGATGGATTATAGTA<u>GG</u>	GGATATTAAAAAAAGGGGGTAAAATTGTACATCG CAAAAGGATGAGGAGTCATTTAATTCATCTTACTA TAATCCATCTCTTCAGGTGGAGTCGAGTCCAAGA AGTGGGTTTGGAATTGGCTTTCCAGATCCGGCT CCTTCATTCTCTTCATCGAACTCTTCCACTTCCTT CTCCTTCTGCTCTTTTCTCTTCTTGTT	(f)TTTCTCCAGGAGTGGTTATCG (r)ACATCGCAAAAGGATGAGGAG
cosa-1::3xflag	*UMM-S57-3.22-mRNA-1*	*PPA23791*	*ie1003*	CTTTATTCTTCATTTTACAG<u>TG</u> <u>G</u>	GATCATCCCAGGGAGAGAACGACCTACCCAAAC AGAGATCATAGATCTAATTATCCACTGGGAGCCG GATCTGATTATAAAGACCATGATGGAGACTATAAG GATCACGATATTGATTACAAAGACGATGATGATAA ATAAAATGAAGAATAAAGAGTATTAAATTTATGTTT GTGTTCGTTTTTGTAATTACTGCTTTG	(f)ACGACCTACCCAAACAGAGA (r)CGGATGTGGAAAGACGTACC
dmc-1 mutant	*UMM-S442-1.74-mRNA-1*	—	*ie1005*	TTCGATAAGCTGCTTGGAGG<u>T</u> <u>GG</u>	ATTTAATTGTAACATTCAGACATCCAGTTGATCAA CTAACCTCCGTTATTGCCTGACTTTCGATTCCAC CactagtgTCCAAGCAGCTTATCGAATTCAACACTT CCAGTGGAGATTTTAAAGACTTGCTTGCGTCGT GAACACACT	(f)GGACTCTCGGAGGCTAAAGT (r)ATTCTCGAGCATTGCTTCCT
dmc-1::V5	*UMM-S442-1.74-mRNA-1*	—	*ie1001*	GCAACGTTTGCCATTGCAGC <u>AGG</u>	GATAAAACATGATCTTTTGTCCTTCATAATTGATTA GGTGGAGTCGAGTCCAAGAAGTGGGTTTGGAAT TGGCTTTCCATCCTTTGCATCGACAATTCCTCCT GC**G**GC**G**ATGGCAAACGTTGCTTCGTTCTCAGGC ATATC	(f)TGCCTGAGAACGAAGCAACG (r)ACATGAGATGGCACAAAGGAC
hop-1	*UMM-S341-6.31-mRNA-1*	*PPA10281*				
rad-51 mutant	*UMM-S442-1.74-mRNA-1*	*PPA42255*	*ie1006*	GTCGAGAACGAGGAGAATGC <u>CGG</u>	ATTTATTGGTTACCTCAAGGGACATGATGGACTG GCAGGCGAGTCCGGCATACTAGTTTCTCCTCGT TCTCGACATCAGCGTCGACGTGCGCCATTTGAG CGGACAT	(f)TTCTAGTGACGCGTGTTGTT (r)ACGAATCCTCGTTGCTGAAG

spo-11 mutant	*UMM-S230-10.9-mRNA-1*	*PPA33054*	*ie1004*	ATTCAGAACTTGGCAGAGATCGG	ACAAACATCTTTTTGCACGACAGGATTCTCTCAATCGATCAGTTTCCGATaactagtaCTCTGCCAAGTTCTGAATATGCAAAGATGTCAAGTCAATGTGGTAAGT	(f)GGAAATCCTTCGTTCTCACTATGG (r)GTCTCAATATCAGACAATTTCATTCCG
syp-4::HA	*UMM-S245-8.16-mRNA-1*	—	*ie1002*	GGAGGAGAATTCAACTTCTTCGG	CAAATGGAGGTGGCGGCGGGGGAGGAGGAGAGTTTAATTTTTTTGGTTTTTACCCCTACGATGTCCCAGATTATGCTTAAACCAATTTTTTCGAGCTTGGTGTAATGTATCCA	(f)CCCGTTGATGATGCTACCAG (r)GATACATTACACCAAGCTCGAA

Table S2

Species	Prefix	Source	BioProject
Acanthocheilonema viteae	AVITAE	WormBase ParaSite	PRJEB4306
Acrobeloides nanus	ANANUS	WormBase ParaSite	PRJEB26554
Ancylostoma caninum	ACANIN	WormBase ParaSite	PRJNA72585
Ancylostoma ceylanicum	ACEYLA	WormBase ParaSite	PRJNA231479
Angiostrongylus cantonensis	ACANTO	WormBase ParaSite	PRJEB493
Angiostrongylus costaricensis	ACOSTA	WormBase ParaSite	PRJEB494
Anisakis simplex	ASIMPL	WormBase ParaSite	PRJEB496
Ascaris lumbricoides	ALUMBR	WormBase ParaSite	PRJEB4950
Ascaris suum	ASSUUM	WormBase ParaSite	PRJNA62057
Auanema rhodensis	ARHODE	-	PRJEB29492
Brugia malayi	BMALAY	WormBase ParaSite	PRJNA10729
Brugia pahangi	BPAHAN	WormBase ParaSite	PRJEB497
Bursaphelenchus xylophilus	BXYLOP	WormBase ParaSite	PRJEA64437
Caenorhabditis elegans	CELEGA	WormBase ParaSite	PRJNA13758
Caenorhabditis monodelphis	CMONOD	caenorhabditis.org	PRJEB7905
Cylicostephanus goldi	CGOLDI	WormBase ParaSite	PRJEB498
Dictyocaulus viviparus	DVIVIP	WormBase ParaSite	PRJNA72587
Diploscapter coronatus	DCORON	WormBase ParaSite	PRJDB3143
Diploscapter pachys	DPACHY	WormBase ParaSite	PRJNA280107
Dirofilaria immitis	DIMMIT	WormBase ParaSite	PRJEB1797
Ditylenchus destructor	DDESTR	WormBase ParaSite	PRJNA312427
Dracunculus medinensis	DMEDIN	WormBase ParaSite	PRJEB500
Drosophilae melanogaster	DMELAN	Ensembl	BDGP6
Elaeophora elaphi	EELAPH	WormBase ParaSite	PRJEB502
Enterobius vermicularis	EVERMI	WormBase ParaSite	PRJEB503
Globodera pallida	GPALLI	WormBase ParaSite	PRJEB123
Globodera rostochiensis	GROSTO	WormBase ParaSite	PRJEB13504
Gongylonema pulchrum	GPULCH	WormBase ParaSite	PRJEB505
Paragordius varius	GORDSP	-	-
Haemonchus contortus	HCONTO	WormBase ParaSite	PRJEB506
Haemonchus placei	HPLACE	WormBase ParaSite	PRJEB509
Heligmosomoides bakeri	HBAKEI	-	PRJEB15396
Heterorhabditis bacteriophora	HBACTE	caenorhabditis.org	PRJNA13977
Hypsibius exemplaris	HEXEMP	tardigrades.org	PRJNA360553
Litomosoides sigmodontis	LSIGMO	WormBase ParaSite	PRJEB3075
Loa loa	LOALOA	WormBase ParaSite	PRJNA246086
Meloidogyne hapla	MHAPLA	WormBase ParaSite	PRJNA29083
Meloidogyne incognita	MINCOG	WormBase ParaSite	PRJEA28837
Mesorhabditis belari	MBELAR	caenorhabditis.org	PRJEB30104
Necator americanus	NAMERI	WormBase ParaSite	PRJNA72135
Nippostrongylus brasiliensis	NBRASS	WormBase ParaSite	PRJEB511
Oesophagostomum dentatum	ODENTA	WormBase ParaSite	PRJNA72579
Onchocerca volvulus	OVOLVO	WormBase ParaSite	PRJEB513
Oschieus tipulae	OTIPUL	caenorhabditis.org	PRJEB15512
Panagrellus redivivus	PREDIV	WormBase ParaSite	PRJNA186477
Parascaris equorum	PEQUOR	WormBase ParaSite	PRJEB514
Parascaris univalens	PUNIVA	WormBase ParaSite	PRJNA386823
Parastrongyloides trichosuri	PTRICH	WormBase ParaSite	PRJEB515
Plectus murrayi	PMURRA	ngenomes.org	-
Poikilolaimus oxycercus	POXYCE	caenorhabditis.org	-
Pristionchus exspectatus	PEXPEC	WormBase ParaSite	PRJEB6009
Pristionchus pacificus	PPACIF	WormBase ParaSite	PRJNA12644
Ramazzottius varieornatus	RVARIE	tardigrades.org	PRJDB1451
Rhabditophanes sp. KR3021	KR3021	WormBase ParaSite	PRJEB1297
Soboliphyme baturini	SBATUR	WormBase ParaSite	PRJEB516
Steinernema carpocapsae	SCARPO	WormBase ParaSite	PRJNA202318
Steinernema scapterisci	SSCAPT	WormBase ParaSite	PRJNA204942
Strongyloides ratti	SRATTI	WormBase ParaSite	PRJEB125

Species	***Prefix***	***Source***	***BioProject***
Strongyloides venezuelensis	SVENEZ	WormBase ParaSite	PRJEB530
Strongylus vulgaris	SVULGA	WormBase ParaSite	PRJEB531
Syphacia muris	SMURIS	WormBase ParaSite	PRJEB524
Teladorsagia circumcincta	TCIRCU	WormBase ParaSite	PRJNA72569
Tetranychus urticae	TURTI	WormBase ParaSite	PRJEA71041
Thelazia callipaeda	TCALLI	WormBase ParaSite	PRJEB1205
Toxocara canis	TCANIS	WormBase ParaSite	PRJEB533
Trichinella nativa	TNATIV	WormBase ParaSite	PRJNA179527
Trichinella spiralis	TSPIRA	WormBase ParaSite	PRJNA12603
Trichuris muris	TRMURI	WormBase ParaSite	PRJEB126
Trichuris suis	TRSUIS	WormBase ParaSite	PRJNA179528
Wuchereria bancrofti	WBANCR	WormBase ParaSite	PRJEB536

Table S3

Software	*Version*	*Relevant parameters*
catfasta2phyml	-	-c -f
edgeR	3.18.0	
HTSeq	0.6.1	
IQ-TREE	1.6.10	-bb 1000 -bb -m GTR20+G
MAFFT	7.407	--auto
NCBI-BLAST+	2.5.0+	blastp
OrthoFinder	2.2.7	-og
PhyloTreePruner	20150918	35 0.9 u
Priism	4.7.1	
R	3.5.1	
softWorx	7.0.0	
STAR	2.5.2	--outFilterType BySJout --outFilterMultimapNmax 20 --alignSJoverhangMin 8 --alignSJDBoverhangMin 8 --outFilterMismatchNmax 999 --outFilterMismatchNoverReadLmax 0.04 --alignIntronMin 20 --alignIntronMax 1000000 --alignMatesGapMax 1000000
StringTie	1.3.3	-p 10 -m 50 --rf -f 0.1 -a 10 -j 5 -c 2.5
Transdecorder	3.0.1	
trimAl	v1.4.rev15	-gt 0.8 -st 0.001 -resoverlap 0.75 -seqoverlap 80